

Award Accounts

The Chemical Society of Japan Award for Young Chemists for 2005

Formation of Large Molecular Cluster Anions and Elucidation of Their Electronic Structures

Masaaki Mitsui*[1] and Atsushi Nakajima*[1,2]

[1]Department of Chemistry, Faculty of Science and Technology, Keio University, 3-14-1 Hiyoshi, Kohoku-ku, Yokohama 223-8522

[2]CREST, Japan Science Technology Agency, c/o Department of Chemistry, Keio University, Yokohama 223-8522

Received November 30, 2006; E-mail: mitsui@sepia.chem.keio.ac.jp

The present account describes our efforts to understand the microscopic aspects of condense phase phenomena, such as ion solvation in molecular liquids and charge carrier localization in molecular solids, by viewing finite-size molecular clusters as their embryonic forms. In this effort, we efficiently prepared supersonically cooled, isolated molecular cluster anions with up to more than 100 constituent molecules and size-selectively investigated their electronic structures using anion photoelectron spectroscopy. Large anionic clusters of two different types of organic molecule; acetonitrile and naphthalene reported as examples of the noteworthy results obtained in our studies. In these two systems, we found that energetically close anionic isomers coexist over a broad range in size, and their contribution in the photoelectron spectra could be separated using anion beam hole-burning technique. A detailed inspection into the electronic states and size-dependent energetics of each isomer has enabled us to establish a link from the large finite cluster to the infinite bulk system.

Molecular clusters are finite aggregates consisting of 2–10^4 molecules and have been regarded as an excellent model system to use for gaining profound insights into weak noncovalent interactions, which play a predominant role in determining the structures and properties of molecular assemblies in chemistry, biology, and soft-material science. In molecular clusters, most of the properties originate from weakly perturbed, easily recognized, and well-defined units. Additionally, the finite number of molecules in the gas phase under collision-free conditions makes a theoretical treatment much easier than that of bulk liquids and solids. Over the last two decades, therefore, intensive experimental and theoretical studies on molecular clusters have been performed, and a large number of review articles on the spectroscopic study of molecular clusters have been published in last twenty years.[1–22]

A main subject of research on molecular clusters is to explore the gradual evolution of the structural, electronic, thermodynamic, and chemical properties from molecular to condensed matter systems in a step-by-step manner, since the number of molecules making up the cluster (i.e., cluster size or n) can be varied successively. In addition, the macroscopic asymptotes ($n \rightarrow \infty$) can be obtained by extrapolating the experimental data for the clusters up to very large n.[6] In order to fully take advantage of this potentiality of the cluster approach, size-selective investigations on a broad size range of molecular clusters has been deemed imperative.

Heretofore, various types of laser-based spectroscopic methods with size-selectivity have been developed and mainly applied for molecular clusters with less than 10 molecules. Nowadays, size-selective spectroscopy of clusters containing 10–1000 molecules is a fascinating and challenging area in the field of molecular clusters, because such studies are expected to provide a significant contribution to probe the "real" transition of the properties of matter from molecular to macroscopic extremes (i.e., molecular liquids and solids). Some previous studies have already addressed this subject. Representative examples are the spectroscopic works conducted around 1990: the electronic spectroscopy of $(benzene)_n$ ($n \leq 60$)[23,24] and $(H_2O)_n^-$ ($n = 6$–50),[25] and the photoelectron spectroscopy of $(H_2O)_n^-$ ($n = 2$–69),[26,27] $(NH_3)_n^-$ ($n = 41$–1100),[27,28] $X^-(H_2O)_n$ ($n = 1$–60),[29,30] and $X^-(CH_3CN)_n$ ($n = 1$–55; X = Cl, Br, and I).[31] In recent years, many beautiful experimental results have been reported for large hydrated clusters, such as SO_4^{2-}-$(H_2O)_n$ ($n = 4$–40),[32] $H^+(H_2O)_n$ ($n \leq 27$),[33–35] and $(H_2O)_n^-$ ($n \leq 200$),[36–39] using the coupling of the state-of-the-art molecular beam sources and optical methods with mass spectrometry. It is further noted that, while no size-selection has been implemented, infrared predissociation spectroscopy of giant water clusters (average sizes; $\langle n \rangle = 20$–1960) has been recently reported by Buck and co-workers.[40]

As just mentioned above, the spectroscopic studies on large-size clusters of small σ-type molecules, like water, has made

Published on the web June 13, 2007; doi:10.1246/bcsj.80.1058

significant progress, but those of π-conjugated organic molecules, such as polycyclic aromatic hydrocarbons (PAHs), remain almost completely undeveloped to date. There are some reasons for this restriction. First, most of these molecules are solid at room temperature, have a relatively high melting temperature and are non-volatile. Thus, it is generally difficult to produce sufficient amounts of their large clusters to implement size-selective spectroscopic investigations. Indeed, almost all previous experimental studies of PAH clusters[41–45] have been limited to the size range of $n \leq 10$. Second, due to the significant improvements in ab initio and density functional theory (DFT) algorithms and rapid progress in computational capability, acceptably accurate theoretical calculations have become available even for larger aggregation systems. However, realization of this is still extremely difficult at present even for the relatively small aggregates of PAHs, because a large number of constituent carbon atoms in the clusters inevitably result in a large basis set number and the importance of many-body effects and electron correlation require very accurate and costly molecular orbital calculations. In this context, we recently succeeded in producing large amounts of cluster anions of many π-conjugated organic molecules, such as benzene,[46,47] oligoacenes,[48] oligothiophenes,[49] and oligophenylenes[50] as well as small organic molecules like and acetonitrile[51] by using an Even–Lavie valve[52] capable of providing very cold molecular beam conditions. Furthermore, we examined their electronic structures with anion photoelectron spectroscopy in a size-selective fashion.[46–51] As discussed later, the improved knowledge about electronic structures of large charged clusters of π-conjugated organic molecules can be extended to gain insight into charge localization, charge transfer, and polarization phenomena in organic molecular crystals.

In this account, we would like to present our efforts to produce large amounts of molecular cluster anions and the application of anion photoelectron spectroscopy to the study of their electronic structures. A number of molecular systems (more than 20 compounds) have hitherto been studied in our work, but this account will focus on some of the most important results among those studies. The organization of this account is as follows. In Section **1**, we will start with a description of the production method of "large" molecular clusters and their anions, including some experimental results obtained in our study. We will also give a description of anion photoelectron spectroscopy as well as anion beam hole-burning photoelectron spectroscopy. In Section **2**, we will present a synopsis of novel experimental findings in large anionic clusters of acetonitrile and naphthalene. Finally, Section **3** is a summary and a discussion of future perspectives.

1. Experimental Methodology

1.1 Production of Large Molecular Cluster Anions. Molecular clusters are usually produced by using supersonic jet expansion into a high vacuum through continuous nozzles or pulsed valves at ambient or elevated temperatures, which is now a very familiar method.[53,54] Therefore, only the salient points pertaining to the production of "large" molecular clusters are explained here. By means of supersonic expansion of a mixture of molecules diluted in a carrier gas (typically a noble gas), both efficient cooling and formation of molecular clusters were easily achieved in the gas phase. As is well known, there are some important factors in the production of large molecular clusters, e.g., the partial pressure of the seed molecules (P_{seed}), the total pressure of the supersonic expansion (P_{total}), the seed ratio ($R_{\text{seed}} = P_{\text{seed}}/P_{\text{total}}$), and the shape of nozzle. To increase the total number of collisions between seed molecules during expansion, it is necessary to obtain a reasonable P_{seed} by heating both the sample reservoir and the valve. Concurrently, a higher P_{total} is needed to sufficiently remove the condensation energy generated in the clustering process. Since neat expansions (i.e., $R_{\text{seed}} = 1$) tend to produce metastable clusters via evaporative cooling and produce a wide energy distribution, they are commonly not preferred to produce cold stable clusters. Hence, the efficient production of internally cold, large molecular clusters necessitates the supersonic expansion at high R_{seed} and with higher P_{seed} and P_{total}.

Even and co-workers[52] have developed a new high-pressure, high-temperature, ultra-short-pulsed valve (Even–Lavie valve), and successfully produced ultracold aromatic molecules with the rotational temperature below 1 K. They have produced He-solvated clusters using this valve.[52,55] High operating pressure (up to 120 bar) and temperature (up to 250 °C) of the Even–Lavie valve make it possible to produce cold molecular beams under adiabatic expansion conditions with a high P_{seed} and P_{total} for a wide variety of molecular systems. It is, thus, very well suited to produce internally cold, large molecular clusters, and we have incorporated this valve with electron attachment sources in order to produce very large molecular cluster anions, as mentioned below.

Determination of the size distribution of clusters is generally implemented by ionization combined with mass spectrometry. In the case of experiments on size-selected cluster ions, ionization process is included in a part of production.[11,13] In the production of cluster anions, a method of electron attachment early in the supersonic expansion is widely used,[3,13] because cluster growth, reorganization, and cooling after electron attachment can be promoted by multiple collisions in the high-density zone of the expanding jet. As depicted in Fig. 1, we employed two anion production methods:[56] (a) injection of slow photoelectrons (kinetic energy: ≈0.3 eV), produced by irradiating the surface of a Y_2O_3 disk with the second harmonics of a Nd^{3+}:YAG laser, and (b) high-energy electron impact ionization method (typically 300 eV, ≈5 mA), where the formation of cluster anions results from attachment of slow secondary electrons (kinetic energy: <1 eV) generated by ionization of the carrier gas. In both methods, electrons were injected into the dense area of the supersonic expansion with the distance (z) between ionization region and nozzle orifice variable from 1 to 50 mm. The cold cluster anions, thus formed, were skimmed into an ion packet, extracted coaxially with a pulsed electric field (−3.0– −5.0 keV) and detected 2.2 m downstream with an in-line Wiley–McLaren time-of-flight mass spectrometer (TOF-MS) with a mass resolution ($M/\Delta M$) ca. 150.

The results of mass spectrometry for so-formed cluster anions are presented as follows. One example is the first successful production of neat benzene cluster anions, $(\text{benzene})_n^-$ in the gas phase.[46,47] Benzene clusters are the simplest prototype aromatic molecules for understanding the fundamental aspects of π–π interactions. An extensive amount of work has

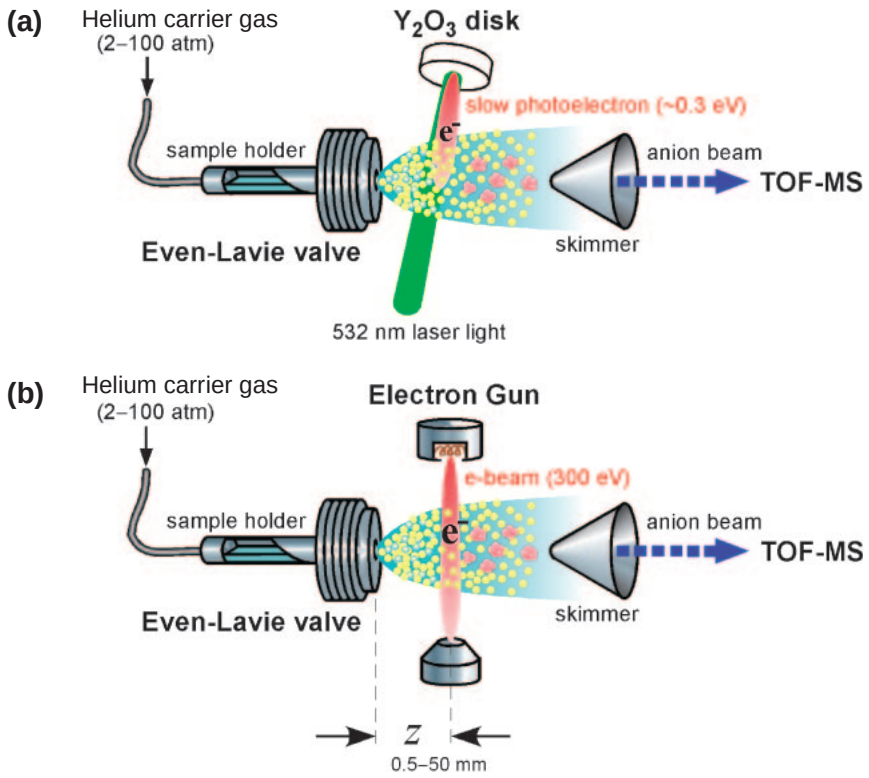

Fig. 1. Two anion production methods employed in this work: (a) injection of slow photoelectrons produced by irradiating the second harmonics of an Nd^{3+}:YAG laser onto a Y_2O_3 disk surface, and (b) high-energy electron impact ionization method where the formation of cluster anions results from attachment of slow secondary electrons generated by inelastic collision with the helium carrier gas.

hitherto been devoted to the spectroscopy and structure of neutral and cationic clusters of benzene;[7,8,22,57–70] however, there has been, to the best of our knowledge, no report on anionic clusters of benzene. As is well known, a benzene molecule has a negative electron affinity (EA); for example, vertical EA $= -1.12$ eV has been reported by electron transmission spectroscopy.[71] The formation of the valence anion of a benzene molecule is thus unfavorable in the gas phase. In contrast, a benzene molecular anion can be stably formed in the condensed phases by the solvent-induced stabilization,[72–76] which leads to the following simple question: "How many benzene molecules are needed to bind an excess electron?" An answer for this question is given in Fig. 2, which shows the TOF mass spectrum of benzene cluster anions obtained by injecting low-energy electrons (≈0.3 eV) in benzene vapor at He stagnation pressure of 70 bar. A very large onset of $n = 53$ (see inset of Fig. 2) was observed together with a sharp rising part ($n = 53$–63) and a roughly exponential intensity fall-off with increasing cluster size ($n \gtrapprox 75$). This indicates that the series of the mass distributions is attributed to homogeneous benzene cluster anions, for the following three reasons. 1) Since cluster anions of yttrium monoxide benzene, YO^--$(benzene)_m$ ($m = 0$–60), were simultaneously observed as well, these impurity cluster anions can play an important role in the precise mass assignment, as shown in Fig. 1. Although there is some uncertainty due to low mass resolution, the mass assignment is consistent with the formation of benzene cluster anions within the order of ±1.5 amu. 2) When a disk of zirconium (Zr) was used as the low-energy electron source with the 4th harmonic of

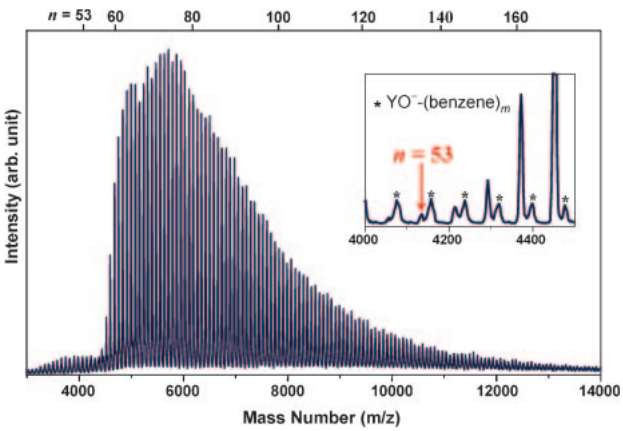

Fig. 2. TOF mass spectrum of $(benzene)_n^-$ ($n = 53$–180) obtained by electron attachment of slow photoelectrons (see Fig. 1a). The inset shows the expanded view of threshold size ($n = 53$) of $(benzene)_n^-$ clusters with the peaks (∗) of yttrium monoxide benzene, YO^-–$(benzene)_m$.

Nd^{3+}:YAG (4.66 eV), the same spectrum was obtained. This evidently indicates that no impurities coming from the Y_2O_3 disk contribute to the series of the mass peaks in question. 3) This is decisively confirmed by the results of photoelectron measurements. The vertical detachment energies (VDEs) of $(benzene)_{53–124}^-$ are 0.4–0.6 eV, while those of YO^--$(benzene)_m$ (even at small m) are more than 1.0 eV. Furthermore, a possibility of a proton-loss product, phenyl radical

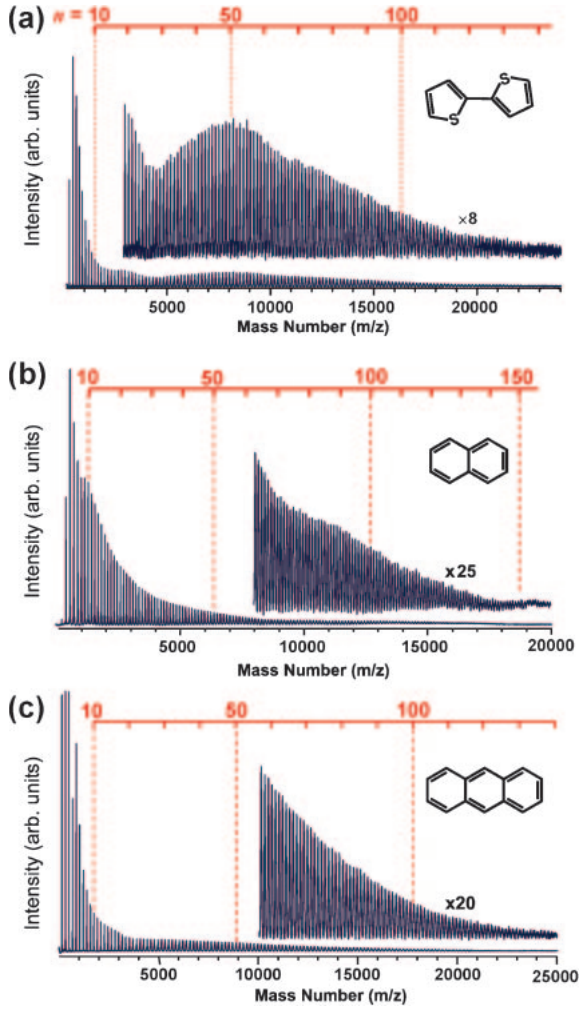

Fig. 3. TOF mass spectra of (a) 2,2-bithiophene, (b) naphthalene, and (c) anthracene cluster anions, obtained by high-energy electron impact ionization (see Fig. 1b).

anion ($C_6H_5^{\bullet-}$) solvated by benzene molecules, can be excluded as well, because EA of $C_6H_5^{\bullet-}$ is known to be $\approx$1.1 eV,[77] which is much larger than the VDEs of $(benzene)_{53-124}^-$.

The threshold size (n_{th}) for continuous formation of abundant series of benzene cluster anions ($n_{th} = 53$) is much larger than those of other anionic cluster systems, e.g., $(pyridine)_n^-$ ($n_{th} = 4$),[78,79] $(H_2O)_n^-$ ($n_{th} = 11$),[11,13,80] $(CH_3CN)_n^-$ ($n_{th} = 13$),[81] and $(NH_3)_n^-$ ($n_{th} = 35$).[82,83] The very large n_{th} of $(benzene)_n^-$ suggests a crucial importance of many-body polarization effects beyond the first solvation layer to fully stabilize excess electrons in benzene aggregates. However, it should be noted that the threshold size observed experimentally often strongly depends on the formation method of the cluster anions. In the electron attachment process, in general, a considerable amount of excess energy is imparted to the clusters, and this energy may be rapidly dissipated into the dense manifold of intermolecular, vibrationally excited states of a cluster, causing reorganization, evaporative cooling, and/or fragmentation of the cluster during the expansion. In addition, these processes might produce metastable anionic species surviving until the detection where their neutral forms have a negative adiabatic EA. Indeed, by using the high-energy electron impact method, smaller benzene cluster anions with $n < 53$ are produced together with the larger $(benzene)_{n\geq 53}^-$ clusters,[46,47] suggesting the occurrence of such phenomena.

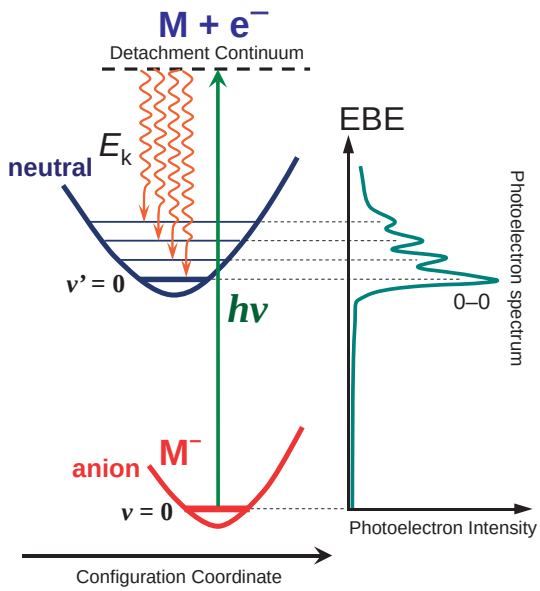

Fig. 4. Scheme of the photodetachment transition in anion photoelectron spectroscopy. The right side, the corresponding photoelectron spectrum are displayed. Notice that the 0–0 transition represents EA_a or ADE.

Figure 3 shows the mass spectra of cluster anions measured for three aromatic compounds, that is, 2,2-bithiophene (2T),[49] naphthalene (Nph), and anthracene (Ac), which are solid at room temperature and have different melting points (2T: 33 °C, Nph: 81 °C, Ac: 216 °C). The cluster anions were formed by expanding sample vapor seeded in 30–100 bar He-carrier gas into a vacuum chamber and subsequent high-energy electron impact ionization. In the case of 2T, continuous formation of 2T cluster anions, $(2T)_n^-$ from $n = 1$ to 150 was clearly observed in the mass spectrum (Fig. 3a). In our TOF-MS measurement, the detectable mass was limited to $\leq$25000 u (i.e., $(2T)_n^-$ with $n \lessapprox 150$) due to lower velocities of larger cluster anions and limited sensitivity of ion detector. In the photoelectron measurement, however, a weak photoelectron signal was detected up to $n \approx 500$, suggesting the formation of $(2T)_n^-$ clusters with value of n of 500 (ca. 80000 u). For both Nph and Ac systems, the cluster anions over $n = 100$ can be also efficiently produced, as shown in Figs. 3b and 3c, which are much larger than the cluster anions formed in the past studies.[44,84]

1.2 Anion Photoelectron Spectroscopy. Photoelectron spectroscopy of anions is conducted by crossing a mass selected beam of anions with a fixed-wavelength laser light ($h\nu$) and measures the kinetic energy (E_k) of the resultant photodetached electrons. Figure 4 illustrates the principle of anion photoelectron spectroscopy, based on photodetachment from an anion ground state to a neutral one. Like conventional photoelectron spectroscopy, it is a direct approach to measure the electron binding energy (EBE), since it relies on the energy conserving relationship $h\nu = EBE + E_k$. The outstanding virtues of anion photoelectron spectroscopy are its capability

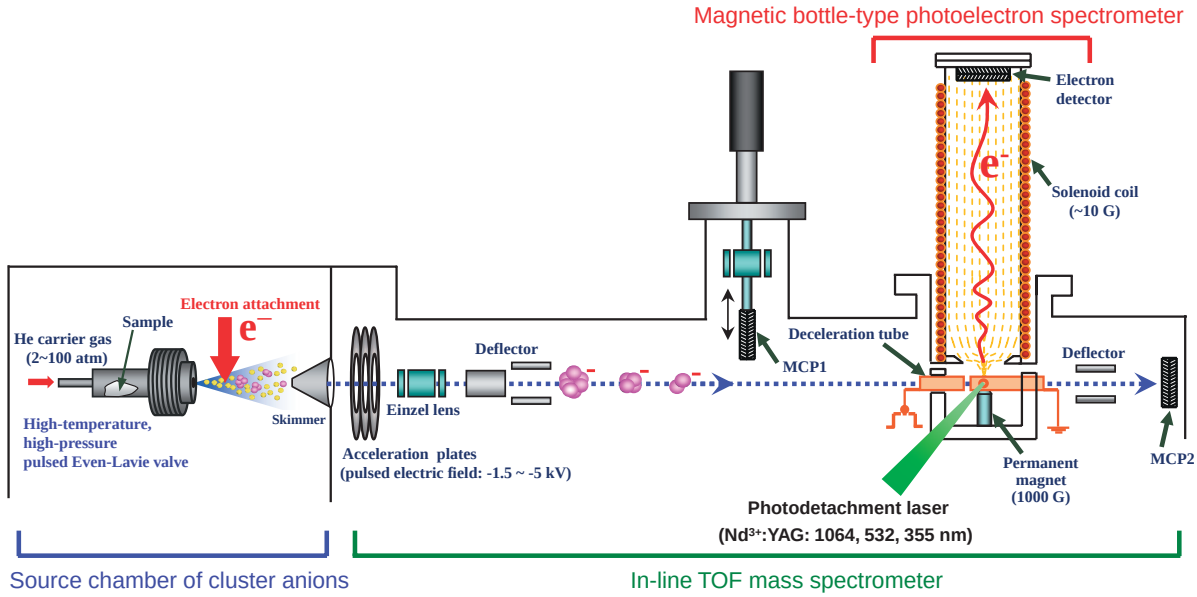

Fig. 5. Schematic diagram of our anion photoelectron spectroscopy apparatus with an in-line Wiley–McLaren TOF mass spectrometer and a magnetic-bottle-type photoelectron spectrometer.

1) to allow mass selection prior to photodetachment, which is extremely difficult in conventional photoelectron spectroscopy via cation ← neutral transitions, 2) to measure directly the electron affinities of isolated molecules[13,85–90] and their clusters with a high precision, and 3) to probe the excited states of neutral molecules.[13,85–89] In particular, the "dark" optically forbidden electronic states (e.g., excited triplet states) of neutral molecules are accessible via a one-electron photodetachment transition from the corresponding anion ground state.

Figure 5 illustrates a schematic diagram of our anion photoelectron spectroscopy apparatus[56,91] which consists of three parts: a cluster anion source, an in-line Wiley–McLaren TOF-MS ($M/\Delta M \approx 200$), and a magnetic-bottle-type electron energy analyzer.[92] On the left side, the anion source containing a pulsed Even–Lavie valve and electron gun (or Y_2O_3 disk) is displayed, the details of which have been already mentioned above. The cluster anions formed in the source chamber continue through a skimmer to the ion flight tube for the linear TOF-MS, where a pulsed electric field directs the cluster anions toward a magnetic bottle photoelectron spectrometer. TOF mass spectrum of the cluster anions was measured at two different positions depending on the experimental aims. To obtain a higher quality mass spectrum, we used the up-and-down movable micro channel plate detector (MCP1) put in front of the magnetic bottle TOF spectrometer (thus avoiding the loss of ions due to a magnetic field). On the other hand, when we performed the mass-selected photoelectron spectroscopy measurements, we used another MCP detector (labeled as MCP2) located at the back of the magnetic bottle photoelectron spectrometer.

When the target anions reach the magnetic bottle, they are photodetached with 1064 nm (1.165 eV), 532 nm (2.331 eV), or 355 nm (3.496 eV) of a Nd^{3+}:YAG laser. In the measurements for cluster anions with the mass less than 4000 u, the anions accelerated by a pulsed electric field of −1.5 keV were decelerated to minimize the degradation in energy-resolution arising from a Doppler effect that causes the energy of the detached electron to spread. The resultant energy resolution was about 50 meV for 1 eV photodetached electrons. Meanwhile, the larger cluster anions with ≥4000 u have relatively lower velocities, irrespective of high acceleration voltage (E_I) of ≈4 keV, and the Doppler broadening[93] has been, for example, estimated to be ca. 90 meV at $E_k = 1$ eV for 4000 u or ca. 40 meV at $E_k = 1$ eV for 25000 u (at $E_I = 4$ keV). These values are similar to our instrumental resolution (i.e. ca. 50 meV at $E_k = 1$ eV) attained by ion deceleration. Indeed, the photoelectron spectral feature for the large mass anions (≥4000 u) did not changed by varying the acceleration voltage from −1.5 to −5 keV. Hence, the photoelectron spectra for the large cluster anions were measured without ion deceleration. The detachment laser fluence was kept below 10 mJ cm^{-2} per pulse during the entire measurement so as to avoid possible multiphoton processes. Under these conditions, photoelectron spectra having relatively high signal-to-noise ratios are usually obtained over the range of $n = 1$–100 by the accumulation of 2000–30000 laser shots at 10 Hz repetition rate. The photoelectron spectrometer was calibrated with the $^1S_0 \rightarrow {}^2S_{1/2}$ and $^1S_0 \rightarrow {}^2D_{5/2}$ transitions of the gold atomic anion, Au^-.[94]

1.3 Anion Beam Hole-Burning Experiment. Even with size selection, there is often more than one species (i.e. isomers) contributing to the signal at a given size, requiring additional dissection of the observed photoelectron spectra. In most cases, isomers have different electron binding energies one another, so that they are often observed as plural distinct bands in the photoelectron spectrum. In this case, one can employ an anion beam hole-burning technique so as to verify whether the observed bands originate from different anionic isomers or not. First application of this technique has been reported by Tsukuda et al.[95] for $(CO_2)_6^-$, showing that the $(CO_2)_6^-$ cluster fluctuates between two isomeric forms of CO_2^--$(CO_2)_5$ and $C_2O_4^-$-$(CO_2)_4$. More recently, Akin and Jarrold[96] have applied this method for $Al_3O_3^-$, where two structural isomers:

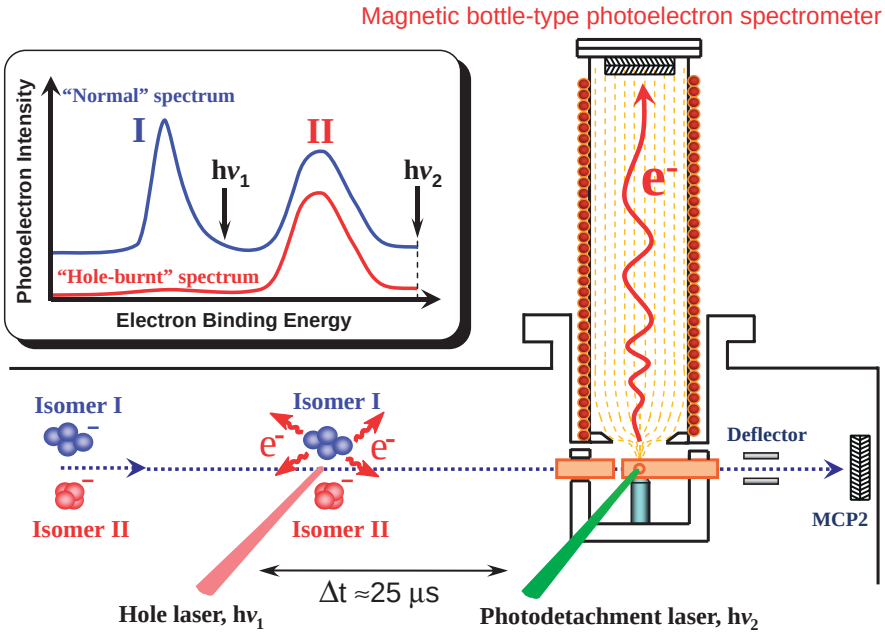

Fig. 6. Experimental setup of anion beam hole-burning photoelectron spectroscopy. As exemplified in the inset, if EBE of isomer I is much lower than that of isomer II and if no transformation between two isomers takes place on the timescale of the measurement, the lower EBE "isomer I" can be selectively photodetached by using the HB laser ($h\nu_1$). After the photodetachment by the HB laser, the remaining anions enter the magnetic bottle spectrometer, where the "Hole-burnt" photoelectron spectrum is measured by intersecting the photodetachment laser ($h\nu_2$). The two laser pulses were temporally separated from each other by ≈25 μs.

the kite-shaped isomer coexists with the bent rectangle isomer having a higher electron affinity.

The experimental scheme for anion beam hole-burning is illustrated in Fig. 6. As shown in the inset of Fig. 6, if EBE of isomer I is much lower than that of isomer II and if no transformation between two isomers takes place on the timescale of the measurement, the lower EBE "isomer I" can be selectively photodetached by using a first laser (hereafter denoted as the HB laser) in the first interaction region. The photodetachment of a fraction of the isomer I in the ion beam by the HB laser pulse is ensured by monitoring the resultant fast-neutral clusters. After the photodetachment by the HB laser, the remaining anions and fast-neutral clusters entered the magnetic bottle spectrometer, where the photoelectron spectrum is measured by intersecting the second photodetachment laser pulse. The two laser pulses were temporally separated from each other by ≈25 μs. In order to cause the first photodetachment to be efficient, strong HB laser pulses (1064 nm, up to several hundreds mJ pulse^{-1}, 10 mm diameter) were delivered from a Nd^{3+}:YAG laser, while the <10 mJ pulse^{-1}, 3 mm diameter, second (532 nm) or third harmonic (355 nm) output of another Nd^{3+}:YAG laser was used in the photoelectron measurements. As will be presented in later sections, the anion beam hole-burning experiment was carried out in our study to confirm that the two distinct bands observed in the photoelectron spectra originate from two distinct anionic species.

2. A Link of Electronic Structure from Cluster to Bulk

2.1 Electron Localization in Neat Acetonitrile Systems: Coexistence of Solvated Electron and Covalent Dimer Anion.[51] **2.1.1 Research Background:** Electron localization in molecular liquids has attracted widespread interest largely because of its fundamental importance in physics and chemistry. In general, two different localized forms of electrons are known for molecular liquids. One is a solvated electron (e_s^-) of which the excess electron is cooperatively trapped in a cavity formed by several solvent molecules. The other is a solvent-bound valence anion, of which the extra electron is fully localized on one (or two) solvent molecule(s), i.e., monomer (or dimer) radical anion. e_s^- is well known to be exclusively formed in a wide variety of molecular liquids, for instance, water,[97] ammonia,[98] and alcohols.[99] On the other hand, valence anions can be produced permanently or temporarily in many organic liquids. Although equilibria of e_s^- with solute anions in nonpolar liquids have been known for a long time,[100] cases of neat liquids, in which e_s^- and solvent valence anion stably coexist, are quite rare.

Acetonitrile (CH_3CN) has a large dipole moment (≈4 D) and a negative vertical EA (−2.84 eV) in the gas phase,[101] and liquid CH_3CN is well recognized as one of the most representative polar solvents. In very early studies,[102] it was considered that solvated electrons are produced in liquid CH_3CN, like water. In 1977, however, Bell et al.[103] suggested that the formation of two kinds of valence anions in neat liquid acetonitrile: one absorbing in the IR region at 1–2 μm and the other in the visible at 400–800 nm. They assigned the former and the latter species to be the monomer and covalent dimer anions of CH_3CN, respectively. Recently, this view has been revised by two research groups. Shkrob and Sauer[104] have conducted a definitive study on excess electron localization in liquid CH_3CN using pulse radiolysis-transient absorption and time-resolved photoconductivity methods. A second group, led by Xia et al.,[105] has also studied this system using femtosecond pump–probe spectroscopy. Although different techniques have

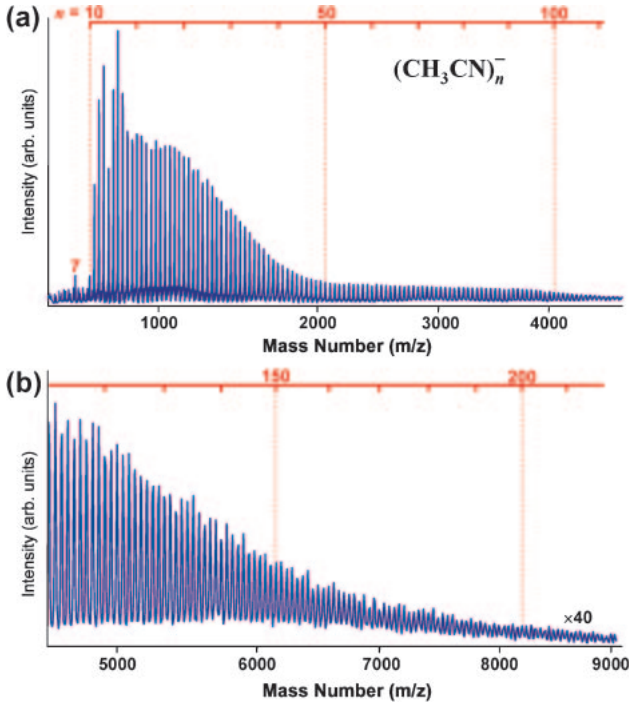

Fig. 7. TOF mass spectra of acetonitrile cluster anions, $(CH_3CN)_n^-$, with (a) $n = 7$, 10–110 and (b) $n > 110$ produced by high-energy electron impact ionization (see Fig. 1b).

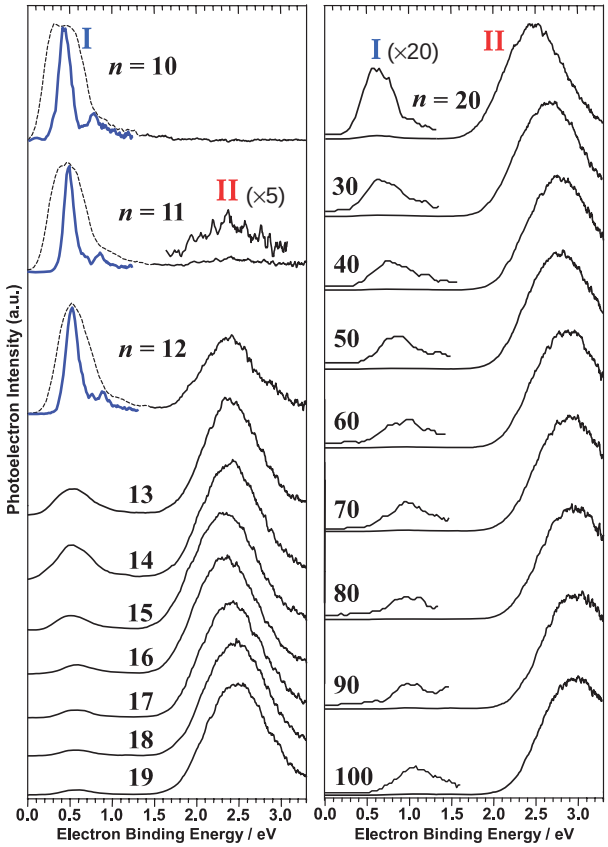

Fig. 8. Photoelectron spectra of $(CH_3CN)_n^-$ (n = 10–100) measured at 355 nm (3.496 eV) without deceleration of parent ions, together with the spectra of n = 10–12 taken at 532 nm (2.331 eV) with deceleration of parent ions. The two anionic isomers are labeled as I and II.

been used by both groups, each has reached the same conclusion, namely, the IR absorbing-species is e_s^- and the visible-absorbing species is the covalent dimer anion of CH_3CN.

In the gas phase, acetonitrile cluster anions, $(CH_3CN)_n^-$, have been also studied by many researchers.[79,81,106,107] The first experimental study of the $(CH_3CN)_n^-$ clusters has been reported by Kondow and co-workers,[81] who found the continuous formation of $(CH_3CN)_n^-$ with $n \geq 13$ by means of collisional electron transfer from high-Rydberg krypton atoms to neutral clusters. As for small clusters, only the odd numbered species ($n = 3$, 5, and 7) have been produced by the Desfrançois and Schermann group using the Rydberg electron transfer (RET) method.[106,107] The peaked Rydberg quantum number dependences of relative formation rate constants for $n = 3$ and 5 demonstrate their dipole-bound characters, though the heptamer anion ($n = 7$) is not a pure dipole-bound species.[107] To our knowledge, however, the excess electron states of the larger $(CH_3CN)_n^-$ clusters have not yet been experimentally elucidated. Currently, it is therefore not clear how the excess electrons states in finite CH_3CN systems evolve into the two different bulk anionic forms, i.e., e_s^- and covalent dimer anion. Elucidation of this point should provide a rationale for the unusual coexistence of e_s^- and valence anion in liquid CH_3CN.

2.1.2 Mass Spectrum of $(CH_3CN)_n^-$: Figure 7a shows the mass region of 50–4700 u of a typical mass spectrum of $(CH_3CN)_n^-$ generated by the electron impact ionization method. The cluster size distribution, in particular in the small cluster size region, is somewhat different from that from the RET method.[80] In our experimental conditions, an abrupt increase in ion intensity was always observed from $n = 10$, together with very weak signals for $n = 2$–9 (note that $n = 7$ is the most abundant size formed), of which their appearances were extremely sensitive to source conditions. Hence, the anions with $n = 2$–9 (except for $n = 7$) may be kinetically stable anionic species, which are presumably produced by evaporative cooling and/or fragmentation of larger clusters during the expansion. The clear onset at $n = 10$ of the abundant series most likely suggests the emergence of a new anionic state in the larger cluster anions. As shown in Fig. 7b, the efficient production of very large $(CH_3CN)_n^-$ clusters over $n = 200$ was also observed under intense expansion conditions of 50–100 bar He-carrier gas.

2.1.3 Photoelectron Spectra of $(CH_3CN)_n^-$ (n = 10–100): Figure 8 shows photoelectron spectra of $(CH_3CN)_n^-$ with $n = 10$–100 taken using a photodetachment laser at 355 nm, together with the spectra of $n = 10$–12 taken at 532 nm with deceleration of the parent ions. In the 532 nm photodetachment spectra of $n = 10$, a strong narrow peak was observed around 0.43 eV, following a much weaker peak at ≈0.8 eV, which was not resolved in the lower energy-resolution spectra at 355 nm. Since the energy spacing between these two peaks was very close to the energy of C–H stretching vibrations, we tentatively assigned the two peaks to the origin-containing peak and to the excitation of C–H stretching modes. A similar assignment was also made with respect to the spectra of $n = 11$ and 12. As

illustrated in Fig. 8, we hereafter denote the two peaks as "band I."

A noticeable change was found in the spectra as the cluster size increased. For $n = 10$, only band I was observed. Interestingly, for $n = 11$, another very weak band (denoted by "II") appeared at much higher energy (≈2.4 eV). The relative peak intensities between bands I and II were completely reversed for $n = 13$, and the peak intensity of band II increased preferentially with n. However, band I did not completely disappear in the larger clusters, and band I barely was observed even to $n > 100$. The relative intensities of band I to band II did not change markedly on moving to $n \gtrapprox 30$. The values of VDE—the energy required to remove the excess electron vertically—of band I shifted gradually with increasing cluster size, as did those of band II. Another remarkable feature is the large difference in electron binding energy between bands I and II. The coexistence of two different anionic isomers has been reported for several cluster anions, such as (uracil)$^-$Xe,[108] (pyridine)$_4^-$,[78,79] and (HF)$_3^-$,[109] in which the differences between VDEs of the isomers have been reported to be ≈0.2 eV. For the $(CH_3CN)_n^-$ clusters, however, the differences between VDEs of bands I and II (≈1.8 eV at $n = 11$–100) are much larger than in these species. These results illustrate the following three points: (1) two different types of anionic isomers coexist in $(CH_3CN)_n^-$ with $n \geq 11$ and their relative abundances switch drastically in the very narrow size region of $n = 10$–13, (2) a large activation barrier seemingly exists between the two anion states, and (3) the nuclear rearrangement from the corresponding neutral cluster is much more significant in the anion state of band II than that of band I.

2.1.4 Experimental Evidence for Isomers: To verify the above-mentioned three facts experimentally, we employed the anion beam hole-burning technique that was described in the Section **1.3**. Band I (e.g., VDE of $n = 12$ is 0.53 eV) was so widely separated from band II (e.g. VDE of $n = 12$ is 2.38 eV), that the anions yielding band I were selectively photodetached by a 1.165 eV (1064 nm) HB laser pulse. After the photodetachment, they entered the magnetic bottle, and the photoelectron spectrum was measured at 355 nm. Figure 9 shows typical results of photoelectron spectra for $n = 12$ and 13 with and without the HB laser (1064 nm). Complete loss of band I was observed for all of the cluster anions examined here ($n = 11$–30), which confirms that bands I and II originate from different anionic isomers. Besides, it indicates no transformation between two anion isomers, which is probably due to the large activation barrier between these two anionic states as well as low internal temperatures of the produced cluster anions, prohibiting solvent rearrangements.

2.1.5 Electronic States of the Coexisting Two Isomers: Figure 10 shows the photoelectron spectra of $n = 13$ measured at different laser fluence under the same ion source condition. For clarity, they are normalized to the peak intensity of band II. At a high laser fluence (≈100 mJ pulse^{-1} cm^{-2}), the intensity of band I increased nearly 2-fold, compared to that of the spectrum recorded at much lower laser fluence (5 mJ pulse^{-1} cm^{-2}). This laser fluence dependence suggests that the photodetachment cross section (PDCS) of the anion state yielding band I is smaller than that of the anion state

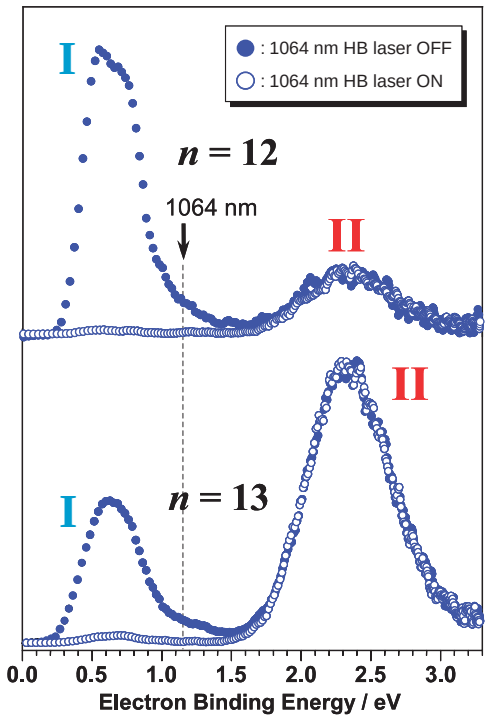

Fig. 9. Photoelectron spectra of $(CH_3CN)_n^-$ with $n = 12$ and 13 measured with (○) and without (●) 1064 nm (1.165 eV) hole-burning (HB) laser prior to the photoelectron measurements at 355 nm. The arrow indicates the maximum electron binding energy accessible with 1064 nm HB laser.

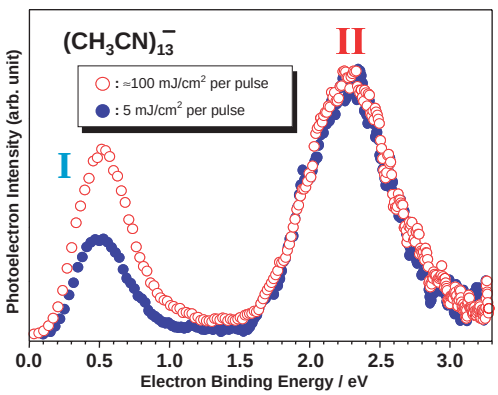

Fig. 10. Photoelectron spectra of $(CH_3CN)_{13}^-$ measured at a high laser fluence (○: ≈100 mJ pulse^{-1} cm^{-2}) and at low laser fluence (●: 5 mJ pulse^{-1} cm^{-2}) under the same ion source condition.

of band II.

To gain further insights into these two anionic states, we evaluated the relative PDCS for bands I and II in the clusters with $n = 11$ and 30, respectively. At $n = 11$, band II was too small to measure its relative PDCS, and so, only that for band I could be measured. In contrast, for $n = 30$ (see Fig. 8), band II was dominant, and only the relative PDCS for band II could be measured. The results are shown in Fig. 11. Even though the threshold detachment region of band I was not examined, it is apparent that the PDCS of band I for $n = 11$ sharply de-

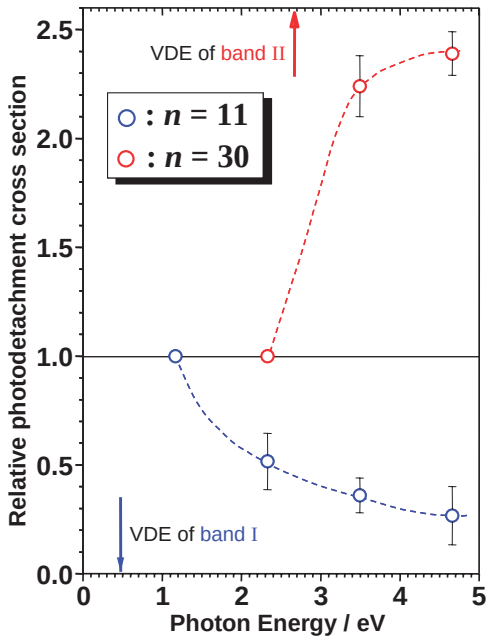

Fig. 11. Relative photodetachment cross sections of $(CH_3CN)_n^-$ with (○) $n = 11$ and (○) 30. The down and up arrows indicate the vertical detachment energies (VDE) of the band I in $n = 11$ and of the band II in $n = 30$, respectively. The dash lines linking each data point are guide for eye.

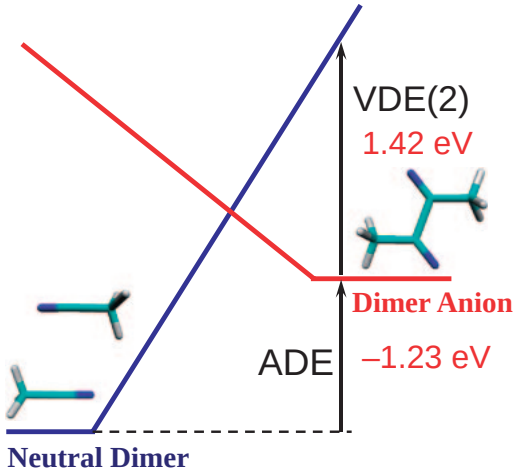

Fig. 12. Schematic energy diagram for neutral and anionic CH_3CN dimer obtained at B3LYP/6-311G(d,p), together with their minimum energy structures. A similar calculated structure of acetonitrile covalent dimer anion has been also reported in Refs. 104 and 105.

creases with increasing photon energy, manifesting diffuse spatial distribution of the excess electron in a cluster. In the case of the diffuse electron, its wave function spans a much larger volume than that of the neutral core and has no node, whereas the wave function of the detached electron has nodes, which become dense with increasing kinetic energy. Thus, the magnitude of the transition dipole moment integral has a maximum around the threshold detachment energy and decreases with the photon energy, since the overlap integral is canceled out by the fast oscillating wave function of the ejected electron.[110,111] Since the diffuse electron is characteristic to a dipole-bound anion[110] or e_s^- state,[25,111] the anion state of band I can be assigned to either the dipole-bound anion or e_s^- state. In strong contrast to band I, for $n = 30$, a rapid increase in PDCS with photon energy is found for band II. This dependence is often observed for anions in which the excess electron occupies a valence molecular orbital, that is, a covalent anion. In common with the photoionization cross sections of neutral molecules, the PDCS shows a rise around the VDE as the result of integrating the Franck–Condon overlap between the vibrational wave functions for the vibrational modes of the anion ground state and neutral one,[112] where the electronic term of the transition dipole moment can be assumed to be constant over the energy range for a particular electronic state.[113] Hence, we can expect that the anionic state of band II is a covalent anion.

An important observation is that band I exists throughout the broad range of n (10–100) and gradually shifts to higher energy with increasing size. This behavior evidently indicates that the anion state of band I is a e_s^- state, since dipole-bound anions usually exhibit a relatively flat trend in electron binding energy with increase in the cluster size and can survive only at low values of n. Besides, the VDEs of band I (0.5–1.1 eV for $n = 10$–100) are higher than those of dipole-bound anions, which are typically much lower than 0.2 eV.[78,108,109] Consistently, the formation of e_s^- was experimentally confirmed in liquid CH_3CN.[104,105] Recent theoretical study of excess electron attachment to CH_3CN clusters by Takayanagi[114] also supports our assignment. In the e_s^- state, the excess electron is cooperatively trapped in a "solvation cavity" formed by the surrounding CH_3CN molecules. Our observation of excitation of C–H stretching modes by electron detachment indicates that the methyl group of CH_3CN is orientated towards the excess electron and there is strong interaction with its H atoms. This orientation is quite reasonable from the direction of the dipole moment of CH_3CN molecule and also has been predicted theoretically.[114]

As mentioned earlier, the dimer anion is the most stable anionic form in liquid CH_3CN.[104] Since band II becomes the more abundant and stable species with increasing n, it is expected that the anion state of the band II could be the dimer anion. As shown in Fig. 8, band II exhibits bell-shaped broad envelopes with very large VDEs. We note that the spectral shape of the band II is intrinsically broad even in higher energy-resolution (ion deceleration) measurements. Both the broad envelopes and the large VDEs of band II suggest the considerable intramolecular rearrangements induced by electron detachment. Then, the DFT calculations with various basis sets were performed to investigate "bare" covalent dimer anion of CH_3CN using the Gaussian 98 software package.[115] As shown in Fig. 12, for example, a minimum energy structure of the covalent dimer anion at B3LYP/6-311G(d,p) level of theory exhibits a largely bent structure with a CCN angle of $\approx 130°$, which is far from the neutral one having an almost linear CCN. A similar structure has been also reported.[104,105] More importantly, all of the B3LYP calculations with different basis sets employed here, e.g., 6-31G (Ref. 105), 6-31G(d,p), and 6-311G, yielded a large negative adiabatic detachment

energy (ADE)—the energy difference between the equilibrium geometries of anion and neutral ground-states—of ca. −1.2 eV and large positive VDE of ca. 1.4 eV (hereafter denoted as VDE(2)) for the dimer anion. Therefore, the dimer anion could be a kinetically stable species in the gas phase, and the cluster anions with $n = 2$ that were weakly observed in the mass spectrum might be the covalent dimer anion produced by solvent evaporation of larger clusters. The present results strongly suggests that the ADE of the anion state of band II must be nearly zero (or slightly positive) when $n = 11$. Consistently, the sum of the calculated values of VDE(2) (1.4 eV) and −ADE (1.2 eV) for the "bare" covalent dimer anion (2.6 eV) is very close to the VDE of the band II for $n = 11$ (ca. 2.4 eV) (see Fig. 8). This is, of course, a coarse comparison; however, the good agreement supports that the anion state of the band II is due to the covalent CH_3CN dimer anion solvated by neutral CH_3CN molecules. Therefore, the bell-shaped broad envelopes with large VDEs are reasonably attributed to the Franck–Condon effect as the result of the substantial nuclear rearrangement of the covalent dimer anion occurring upon photodetachment. Based on this fact, it is also evident that there is a large gap between ADE and VDE of the dimer anion states when $n \geq 11$. In this case, even though the VDE of band II (i.e., covalent dimer anion state) is much larger than that of band I (i.e., e_s^- state), the dimer anion state is not necessarily energetically more stable than the e_s^- state because the stability is correlated to the adiabatic, not the vertical energy.

2.1.6 Why Do Solvated Electron and Covalent Dimer Anion Coexist in Liquid Acetonitrile?: Our initial interest was to understand why e_s^- and covalent dimer anion coexist in liquid CH_3CN. One of our most interesting findings is that the covalent dimer anion state starts to appear when $n = 11$. This result indicates that the solvation of (at least) nine CH_3CN molecules is necessary to turn the ADE of the covalent CH_3CN dimer anion into a positive value. Owing to the very broad features of band II, an accurate ADE value could not be determined from the photoelectron spectrum. However, it is most likely to be very small and positive, since the ADEs of clusters change only gradually with increasing n. On the other hand, the photoelectron spectrum of the same size indicates that the ADE of the excess electron solvated by 11 CH_3CN molecules (0.3–0.5 eV) is also low, (see the onset or the most dominant peak of $n = 11$ in Fig. 8). Therefore, the energy difference between adiabatic levels of the e_s^- and the dimer valence anion states are probably very small when $n = 11$ and should gradually converge to the bulk value of about 0.5 eV as the cluster size increases.[104] Furthermore, the previous experimental and theoretical studies have shown that 9–11 CH_3CN molecules can nearly complete the first solvation layer for halide ions.[31,116] In the first solvation layer, the strong direct ion (or excess electron)–solvent interaction results in efficient anion (or excess electron) stabilization. In contrast, in the second (and larger) layer(s), solvent molecules do not directly interact with the core charge and hence provide no further substantial stabilization for the anion or excess electron. Hence, it is expected that solvation beyond the first layer will not alter the relative energetic stability between the e_s^- and covalent dimer anion states so greatly. Consequently, the close energy-vicinity of these two electron localized states is maintained in very large clusters and even in bulk, resulting in the unusual coexistence of e_s^- and covalent dimer anion in liquid CH_3CN.

2.2 A New Finding in Polycyclic Aromatic Cluster Systems: Emergence of Rigid, Crystal-Like States in Large Anionic Clusters of Naphthalene.[48] **2.2.1 Research Background:** The electronic structure of organic molecular solids, such as polycyclic aromatic hydrocarbons (PAH) and their related aromatic compounds, has been the object of intensive research for almost a half-century.[117–120] It is directly connected with their optical, dielectric, and charge-transport properties, which are currently utilized for widespread applications in organic light emitting diodes, field effect transistors, photovoltaic cells, and so on. A detailed understanding of the electronic structure of organic molecular solids is therefore of immense interest from both fundamental and practical points of view.

Organic molecular solids are usually characterized by weak van der Waals intermolecular interactions and a small overlap between the wave functions of adjacent molecules and have narrow electronic bands. In other words, an electron (or hole) in organic molecular solids is strongly localized on a single molecule, meaning it is a molecular anion (or cation). As well recognized, such a localized charge does not exist as a free particle, but as a polaron-type quasi-particle—an electron (or hole) "dressed" in the electronic polarization cloud of polarized neighboring molecules,[117–121] and the polarization cloud is believed to extend over 10^4 or more molecules.[121] As depicted in Fig. 13, the polarization effects give rise to so-called "gas-to-solid shift," and the polarization energies P^+ for cations (holes) and P^- for anions (electrons) are the parameters that determine the energy level of the transport gap (E_t) for creating a separated free electron–hole pair. So far, reliable experimental data concerning P^+ of π-conjugated organic solids

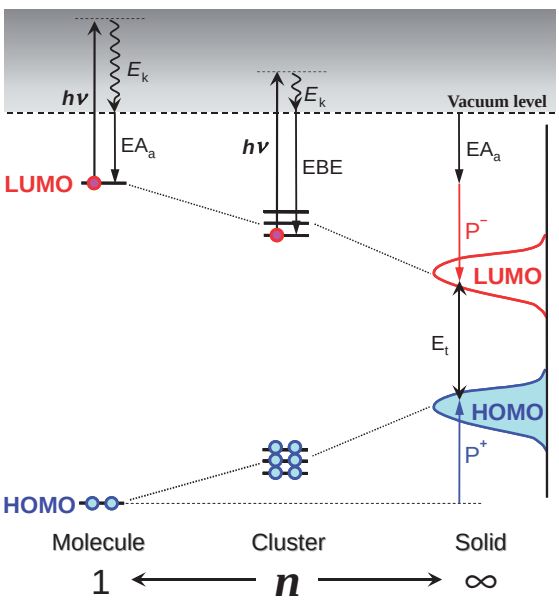

Fig. 13. Schematic energy diagram of electronic structure of an isolated molecular anion, finite cluster anion, and bulk solid. Probing of the excess electron occupying LUMO of cluster anions enables us to explore an energetics of LUMO level from an isolated molecule to the corresponding bulk in a stepwise fashion.

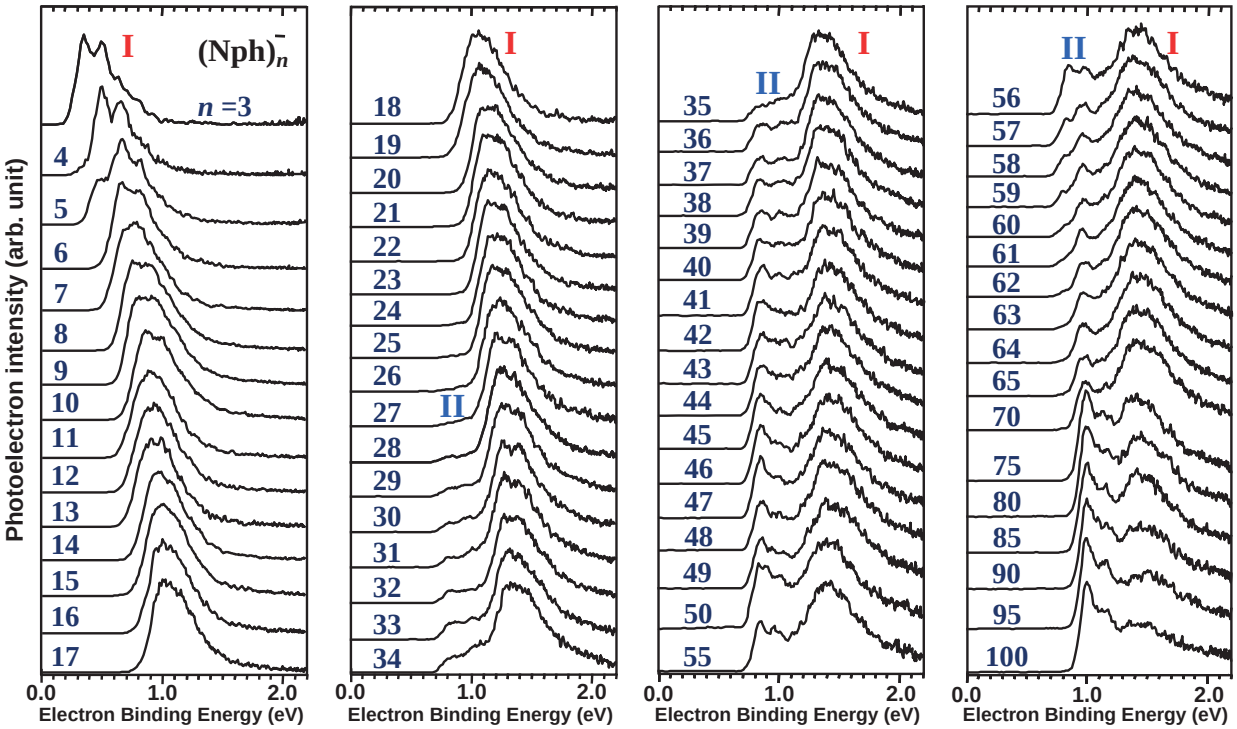

Fig. 14. Photoelectron spectra of naphthalene cluster anions $(Nph)_n^-$ ($n = 3$–100) measured at 532 nm (2.331 eV). Band II started to appear around $n = 28$ and gradually increased in intensity with increasing cluster size. The intensity of band II was extremely sensitive to the cluster ion source conditions, e.g., stagnation pressure and valve temperature including the sample holder. Note that all of the photoelectron spectra were measured under a cold ion source condition which was optimized to maximize the intensity of band II.

has been acquired by using ultraviolet photoelectron spectroscopy (UPS) in the solid state.[122] In strong contrast, there are rather few reliable experimental data for P^-, while it is currently under investigation by means of inverse photoemission spectroscopy (IPES).[123–126]

Finite-size cluster anions of π-conjugated molecules are viewed as an embryo of a negative polaron in organic molecular solids, because the single excess electron doped in the cluster is stabilized by the finite number of polarized molecules, i.e., a finite-size polarization cloud. As shown in Fig. 13, size-selective photoelectron spectroscopy of cluster anions enables us to stepwise explore the energetics of the lowest unoccupied molecular orbital (LUMO) level from an isolated molecule to the bulk. In addition, it provides spectroscopic information about the ion core character (e.g., monomeric or multimeric), and also, it sheds light on the size and geometrical effects on the magnitude of polarization energy. As mentioned above, we were recently able to produce large amounts of cluster anions of many PAHs and their related aromatic compounds and size-selectively investigated their electronic structures by means of anion photoelectron spectroscopy.[46–51] In these experiments, we discovered a novel phenomenon in large-size cluster anions of several PAHs, such as linear oligoacenes.[48] We herein focus on the results involving naphthalene (Nph) cluster anions.

2.2.2 Photoelectron Spectra of Naphthalene Cluster Anions ($n = 3$–100): A single Nph molecule cannot bind an excess electron because of its negative EA_a (−0.19 eV).[127] In 2002, Song et al.[44] have reported that the formation of homogeneous Nph cluster anions, $(Nph)_n^-$, begins at $n = 2$. They have measured the photoelectron spectra of $(Nph)_n^-$ and determined VDEs of the clusters in the size range of $n = 2$–7. In the present study, we examined sizes range up to $n = 100$. Figure 14 shows the photoelectron spectra of $(Nph)_n^-$ over the range of $n = 3$–100 measured at 532 nm. From $n = 3$ to 27, a single asymmetric profile was observed in the spectra, and they shifted gradually toward a higher binding energy with increasing cluster size. In the spectra of $(Nph)_{3,4}^-$, partially resolved vibrational structure was observed, which has been already assigned to the ν_4 (181 meV) and/or ν_5 (171 meV) C–C stretching mode.[44] This vibrational structure signifies that the excess electron occupies the LUMO of a (or few) Nph molecule(s) in the cluster anions. However, this vibrational structure gradually becomes unresolvable as the cluster size grows, because the number of (low-energy) intermolecular vibrational modes excited in the photodetachment process increases rapidly with cluster size. Hereafter, this band is referred to as "band I." From $n = 28$ to 100, a new feature (labeled "II") was observed to emerge on lower EBE side of band I. Although a sharp variation of the spectral profile is seen for band II in the size range of $56 \leq n \leq 60$,[128] their VDEs become an almost constant value of 0.99 eV beyond $n = 60$. Finally, this band became more prominent as n increased, especially when $n \geq 70$. It is surprising that vibrational structure resembling that of $(Nph)_{3,4}^-$ is clearly observed for each band in the spectra with $n = 75$–100.

All of the spectra presented in Fig. 14 were measured under relatively high He-carrier gas pressures (typically 50–100 bar),

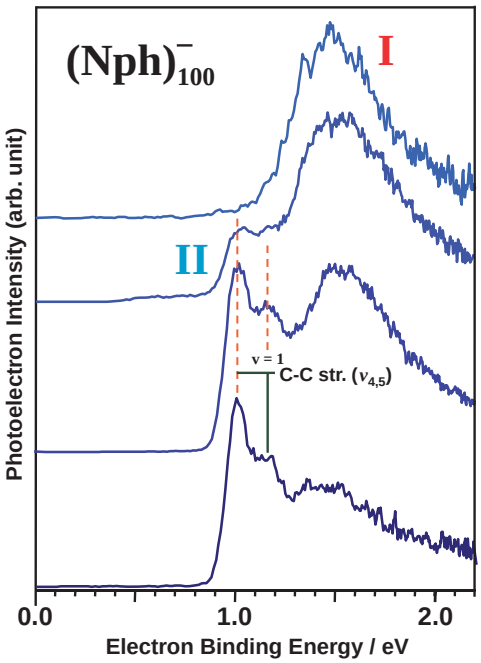

Fig. 15. Photoelectron spectra of $(Nph)_{100}^-$ measured at different He-stagnation pressures. As increasing the stagnation pressure was increased (from top to bottom), band II became more intense than band I and displays the vibrational structure of the C–C stretching mode (ν_4 and/or ν_5).

where we also carefully adjusted the valve temperature, valve opening-time, and the time interval between the opening of the pulsed valve and the high-voltage pulse for the ion extraction, in order to produce colder cluster anions. Note that band II disappears under warmer source conditions, which thus seems to favor colder source conditions. To show clearly this behavior, the effect of varying stagnation pressure is shown for $n = 100$ in Fig. 15. As the stagnation pressure was increased, band II became stronger than band I and clearly exhibited the vibrational structure of the C–C stretching mode of ν_4 and/or ν_5, indicating that more efficient cooling of the cluster ensemble occurs at higher stagnation pressure. The temperature dependence on the cluster source suggests that anionic isomers I and II at a given size are very close in (adiabatic) energy.

The anion beam hole-burning experiments were also carried out, a procedure which distinguishes between anionic isomers having widely differing electron binding energies, as mentioned in Section **1.3**.[95,96] Bands II was sufficiently separated from band I such that the isomer with lower VDE (band II) could be selectively photodetached with the HB laser at 1064 nm (1.165 eV) without detaching electrons from isomer I. After photodetachment, the surviving cluster anions enter the photoelectron spectrometer, where the photoelectron spectrum was measured at 532 nm. Figure 16 shows typical photoelectron spectra for the $(Nph)_{100}^-$ clusters taken with the HB laser off and laser on. As shown in Fig. 16, only band II disappeared with the HB laser ($\approx$50 mJ pulse^{-1}), and no other changes were observed between the spectra with and without the HB laser. This result confirms that bands I and II originate from different anionic isomers, and that there is no dynamic equilibrium between the anion states of isomers I and II on

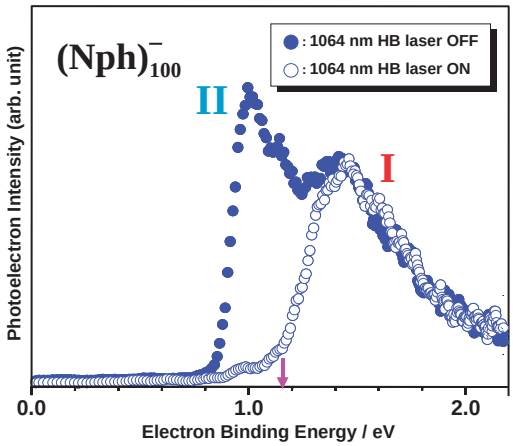

Fig. 16. Photoelectron spectrum of $(Nph)_{100}^-$ measured with (○) and without (●) 1064 nm (1.165 eV) photodetachment prior to the photoelectron measurements at 532 nm. The arrow indicates the maximum electron binding energy accessible with 1064 nm photodetachment.

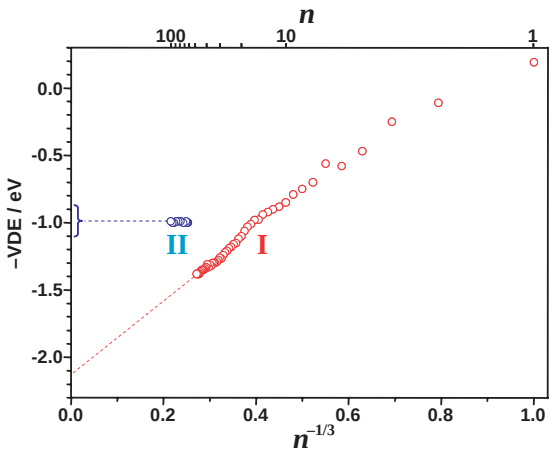

Fig. 17. Plot of −VDEs of isomers I and II as a function of $n^{-1/3}$ where n is the number of Nph molecules. The range of variation in the bulk adiabatic energies of the LUMO level with respect to the vacuum level is also displayed.

the timescale of the measurement.

2.2.3 Insight into Isomers: Comparison to the Bulk: What is different between two distinct anionic isomers? The results of note in this work are that (1) the VDE values of isomer II are nearly size-independent and always 0.5–0.6 eV smaller than those of isomer I, (2) the spectral features of isomer II maintain a relatively sharp profile with an intramolecular vibrational structure, while the spectral profile of band I becomes gradually broader and less structured with cluster size, and (3) colder source conditions favor the formation of isomer II in the size range of $n = 28$–100, whereas warmer conditions favor isomer I in the whole size range examined in this study ($n = 3$–100).

To gain insight into these anionic isomers, we compare the cluster data obtained herein with the bulk data. In Fig. 17, the −VDE values of isomers I and II are plotted against $n^{-1/3}$. The VDEs of isomer I with $n \geq 20$ were fitted linearly and a straight line thus obtained extrapolates to a −VDE(∞) value

of −2.12 eV. In contrast to the size-dependent isomer I, the −VDEs of isomer II in $(Nph)_n^-$ with $n = 60$–100 are not size-dependent, but are nearly constant within experimental uncertainties, i.e., −0.99 eV.

Let us now compare these values with the bulk data to consider the character of these isomers. In molecular crystals, the adiabatic energy of the LUMO level with respect to the vacuum level (hereafter referred to as "E_{LUMO}") is given by $-EA_a + P_{eff}^-$ where P_{eff}^- is the effective polarization energy consisting of the charge-induced dipole interaction and the charge–quadrupole interaction terms. The lattice relaxation energy of oligoacene-type crystals is negligibly small, typically ≈10 meV, a level which is due to the rigidity of the crystal lattice relative to the localized charge.[118,124,126,129] Here, therefore, the contribution of the lattice relaxation energy is ignored. The EA_a of a Nph molecule[127] has been reported to be −0.19 eV. Munn and Eisenstein have theoretically estimated P_{eff}^- of the Nph single crystal to be −1.05 eV.[130,131] On the basis of these data, the E_{LUMO} value was estimated to be −0.86 eV for Nph single crystal. In addition, in the experimental results of IPES for highly ordered Nph thin film on Ag(111) reported by Frank et al.,[123] the energy of the LUMO from the vacuum level has been reported to be -1.1 ± 0.15 eV. Because of image charges on the metal substrate, this energy may be a little larger than the intrinsic energy of the bulk.[126] We will here compare these E_{LUMO} values with the present results.

For isomer I, −VDEs already exceed the bulk E_{LUMO} values in clusters as small as $n \approx 20$, and the extrapolated value of −2.12 eV is much larger than the bulk values (see Fig. 17). This discrepancy indicates that the reorganization energy (λ) considerably contributes to the VDE, i.e., $-VDE = E_{LUMO} - \lambda = -EA_a + P_{eff}^- - \lambda$, where λ is the sum of two reorganization energies: (1) those of the nuclear reorganizations from the equilibrium geometry of the neutral state to that of the anion state and (2) those from the equilibrium geometry of the anion state to that of the neutral state. In other words, the equilibrium geometry of isomer I is far from that of the neutral state. Since isomer I is preferentially produced using warmer sources, electron attachment to relatively warm (or liquid-like) clusters allows for substantial orientational relaxation of neutral molecules around the anion after the electron attachment and result in the anion internalization. This formation process is similar to the cases of the $(H_2O)_n^-$ and $(CH_3CN)_n^-$ clusters, in which the substantial solvent reorganization occurs in the electron internalization process. At this moment, we have no information concerning the cluster structure; however, it is probably far from a highly ordered crystalline form.

On the other hand, the −VDEs of isomer II are size-independent and nearly constant within experimental uncertainties (−0.99 eV; $n = 60$–100). These results indicate that the anion gains only a little stabilization energy by the addition of subsequent molecules. Interestingly, it is found that the near-constant −VDE values of isomers II (−0.99 eV at $n = 60$–100) are very close to the range of bulk E_{LUMO} values (−0.86–−1.1 eV). These energy proximities suggest that the anion state of isomer II correlates to the bulk crystalline state of Nph. In addition, band II, exhibiting an intramolecular vibrational structure, appeared on the lower energy side of band I. In strong contrast to isomer I, the presence of isomer II is evidently due to the anion states being formed without (or with much less) intermolecular geometrical relaxation after electron attachment to the neutral cluster (i.e., $\lambda \approx 0$). This is consistent with the fact that the lattice relaxation energy of the crystal is quite small, only ≈10 meV, owing to the rigidity of the crystal lattice relative to the excess charge.[126,129] Thus, it is conceivable that isomer II is the anionic states arisen from electron attachment to internally cold, crystal-like neutral clusters.

The anion state of isomer II appear to be favorable as the cluster size increases, and besides their near-constant −VDE values (−0.99 eV for $n \geq 60$) are in good agreement with the bulk E_{LUMO} values of Nph crystal (−0.86–−1.1 eV). These facts strongly suggest that isomer II ($n \geq 60$) is the cluster analogue of the "polaron" in the bulk Nph crystal, in which the excess electron accommodated by a single (or few) Nph molecule(s), i.e., the Nph monomer (or multimer) anion core, is stabilized by the remaining, polarized neutral molecules in the cluster. In particular, the energy agreement is a great surprise because the electronic polarization of neutral molecules around the anion is generally believed to extend over 10^4 or more molecules in bulk crystals.[118,121] However, the present observation confirms the considerable localized nature of the electronic polarization around the anion core in the crystal-like cluster. The agreement with the bulk data also suggests that the anion or excess electron is completely incorporated in the internal position of the cluster, i.e. an internalized anion state.[48] To place the anion completely in an internal position in the crystal-like cluster, three or more layers must be stacked in the herringbone-layered motif that is present in Nph crystal. As already mentioned above, the electron attachment process is accompanied by a large amount of excess energy, which can be rapidly dissipated into the dense manifold of intermolecular, vibrationally excited states of a cluster. In the formation process of isomer II, therefore, a thermally activated electron hopping transfer between neighboring Nph molecules in the cluster could perhaps take place through intermolecular π-orbital overlaps in the crystal-like structure and internalize the excess electron without disturbing the intermolecular geometry so greatly. Unlike σ-type molecular clusters (e.g., water and CH_3CN clusters), this might be an electron internalization process unique to the highly ordered clusters of π-conjugated organic molecules. In the future, the interpretation mentioned above should be further verified experimentally and theoretically in relation to the formation process and structural morphology of the crystal-like cluster anions (isomer II) discovered in this study.

3. Summary and Perspectives

In this account, we described the formation of large-size molecular cluster anions and elucidation of their electronic structures by means of size-selective anion photoelectron spectroscopy. Homogeneous anionic clusters of CH_3CN and Nph highlighted as examples of the most striking results obtained in our study. We found for the first time that the different anionic isomers coexist over a broad size range in both the molecular anion systems. For the CH_3CN system, anion photoelectron spectroscopy was used to demonstrate the coexistence of two different anionic species: e_s^- and a covalent dimer

anion of CH_3CN. The distinctly different nature of these two anions was confirmed by using anion beam hole-burning technique and relative photodetachment cross section measurements. This unusual coexistence was attributed to the closely lying nature of their anionic states at just the number of solvent molecules sufficient to almost complete the first solvation layer. On the other hand, the two distinctive anion states, i.e., isomers I and II, were shown to coexist competitively in the large Nph cluster anions. Detailed investigation of the degree of structural rearrangement of the cluster induced by the electron attachment showed that isomer I is a fully relaxed, "disordered" cluster anion formed through the substantial intermolecular reorganization associated with the anion internalization. In contrast, isomer II is a crystal-like cluster anion, which lacks such a geometric relaxation almost entirely, due to their rigidity. From their size-independent VDEs, we concluded that isomer II ($n \geq 60$) is an internalized anion state with a crystal-like structure, which appears to be correlated to negative polaron in the bulk Nph crystal.

As presented in this account, the size-evolution of the electronic structure of cluster anions clearly contains distinct isomers over a broad range of n, and they could be related to the corresponding bulk liquid or solid. However, some important aspects are still unresolved at present. Among these, the most important subject is structural characterization of large aromatic cluster anions, of which the structures were tentatively determined from their electronic structures. For neutral and cationic clusters, structure determination has been performed using various laser-based spectroscopic methods, such as IR–UV double resonance spectroscopy, rotational coherence spectroscopy, and IR multiphoton dissociation spectroscopy. In contrast, structure determination for anionic clusters is much less common and often difficult compared to neutral and cationic species. In the past, vibrational spectroscopy of cluster anions has been implemented by the use of autodetachment[132] or predissociation[133–136] induced by vibrational excitation of the cluster anions. These methods require that the vibrational energy of the excited anion exceeds the electron affinity or the dissociation energy of the cluster anion. However, useful structural information for aromatic clusters often resides in a very low energy region of intermolecular vibrational motions ($\leq 100\,cm^{-1}$).[137] In this regard, stimulated Raman pumping-photoelectron spectroscopy, developed by Neumark and coworkers,[138] may be the most promising spectroscopic method for structural characterization of aromatic cluster anions, although it is still under development for such application. An alternative experimental approach is needed for future progress, because spectroscopic determination of the cluster structure is mostly limited to the cluster sizes feasible for a spectroscopic analysis. Ion mobility spectrometry may be a promising candidate for this purpose, because its capability of the probing geometric structures of PAH cluster ions has been recently demonstrated by Beitz et al.[139] For theoreticians, large aromatic cluster anions can also be rather cumbersome, because their structures are mainly determined by competition between polarization and charge resonance interactions, and the evaluation of charge resonance interaction, in particular, necessitates the application of proper theoretical methodology.[140] In any case, a maximum collaboration between experiment and theory is unequivocally necessary for clarifying this formidable subject in the future.

Finally, it is noted that the coexistence of two isomeric forms in the large Nph cluster anions[48] may imply phase coexistence in the finite-size clusters.[141–143] Although we could not determine the cluster temperature, the variations in the cluster source conditions (see for example Fig. 15) drastically affect the relative abundance of the two distinct anionic isomers. This behavior implies that liquid-like (non-rigid) and solid-like (rigid) neutral clusters temporarily coexist in a supersonic beam (under non-equilibrium conditions), and they are possibly thermodynamically competitive. In larger clusters, a vast number of the internal quantum states, e.g., intermolecular vibrational modes, should be populated at a finite temperature, so that the concept of free energy becomes more important. In the large size regime, therefore, the vibrational entropy contribution to the free energy may dominate the relative abundance of isoenergetic isomers at a given size. Hence, a key step to future progress is to realize the reliable control and measurement of cluster temperature. Also, it is important to obtain experimental information about intermolecular vibrational motions, especially large amplitude intermolecular motions, of the clusters, because they might promote the interconversion between liquid-like and solid-like clusters. In any case, our understanding of these issues is far from complete at present, and we anticipate that our new findings for the very large aromatic cluster anions described in this account will provide an incentive for future works in this domain.

We are grateful to Prof. U. Even and Mr. N. Lavie for a newly designed pulsed-valve. We are also very indebted to people from Nakajima group for doing the experiments: Mr. Shinsuke Kokubo, Mr. Naoto Ando, and Ms. Yukino Matsumoto (Keio University). This work is supported by RFTF (Research for the Future) of Japan Society for the Promotion of Science (JSPS), by Young Scientists (B), No. 14740332 and No. 17750016, and partly supported by Grant-in-Aid for the 21st Century COE program "KEIO LCC."

References

1 L. S. Bartell, *Chem. Rev.* **1986**, *86*, 491.
2 F. G. Celii, K. C. Janda, *Chem. Rev.* **1986**, *86*, 507.
3 A. W. Castleman, Jr., R. G. Keesee, *Chem. Rev.* **1986**, *86*, 589.
4 D. J. Nesbitt, *Chem. Rev.* **1988**, *88*, 843.
5 S. Leutwyler, J. Bösiger, *Chem. Rev.* **1990**, *90*, 489.
6 J. Jortner, *Z. Phys. D: At., Mol. Clusters* **1992**, *24*, 247.
7 P. Hobza, H. L. Selzle, E. W. Schlag, *Chem. Rev.* **1994**, *94*, 1767.
8 P. M. Felker, P. M. Maxton, M. W. Schaeffer, *Chem. Rev.* **1994**, *94*, 1787.
9 H. J. Neusser, H. Krause, *Chem. Rev.* **1994**, *94*, 1829.
10 K. Müller-Dethlefs, O. Dopfer, T. G. Wright, *Chem. Rev.* **1994**, *94*, 1845.
11 A. W. Castleman, Jr., K. H. Bowen, Jr., *J. Phys. Chem.* **1996**, *100*, 12911.
12 S. Sun, E. R. Bernstein, *J. Phys. Chem.* **1996**, *100*, 13348.
13 U. Boesl, W. J. Knott, *Mass Spectrom. Rev.* **1998**, *17*, 275.

14 U. Buck, F. Huisken, *Chem. Rev.* **2000**, *100*, 3863.
15 B. Brutschy, *Chem. Rev.* **2000**, *100*, 3891.
16 H. J. Neusser, K. Siglow, *Chem. Rev.* **2000**, *100*, 3921.
17 C. Desfrançois, S. Carles, J. P. Schermann, *Chem. Rev.* **2000**, *100*, 3943.
18 C. E. H. Dessent, K. Müller-Dethlefs, *Chem. Rev.* **2000**, *100*, 3999.
19 C. Dedonder-Lardeux, G. Grégoire, C. Jouvet, S. Martrenchard, D. Solgadi, *Chem. Rev.* **2000**, *100*, 4023.
20 K. S. Kim, P. Tarakeshwar, J. Y. Lee, *Chem. Rev.* **2000**, *100*, 4145.
21 T. S. Zwier, *J. Phys. Chem. A* **2001**, *105*, 8827.
22 M. O. Sinnokrot, C. D. Sherrill, *J. Phys. Chem. A* **2006**, *110*, 10656.
23 M. Y. Hahn, A. J. Paguia, R. L. Whetten, *J. Chem. Phys.* **1987**, *87*, 6764.
24 D. C. Easter, M. S. El-Shall, M. Y. Hahn, R. L. Whetten, *Chem. Phys. Lett.* **1989**, *157*, 277.
25 P. Ayotte, M. A. Johnson, *J. Chem. Phys.* **1997**, *106*, 811.
26 J. V. Coe, G. H. Lee, J. G. Eaton, S. T. Arnold, H. W. Sarkas, K. H. Bowen, C. Ludewigt, H. Haberland, D. R. Worsnop, *J. Chem. Phys.* **1990**, *92*, 3980.
27 G. H. Lee, S. T. Arnold, J. G. Eaton, H. W. Sarkas, K. H. Bowen, C. Ludewigt, H. Haberland, *Z. Phys. D: At., Mol. Clusters* **1991**, *20*, 9.
28 H. W. Sarkas, S. T. Arnold, J. G. Eaton, G. H. Lee, K. H. Bowen, *J. Chem. Phys.* **2002**, *116*, 5731.
29 G. Markovich, R. Giniger, M. Levin, O. Cheshnovsky, *J. Chem. Phys.* **1991**, *95*, 9416.
30 G. Markovich, S. Pollack, R. Giniger, O. Cheshnovsky, *J. Chem. Phys.* **1994**, *101*, 9344.
31 G. Markovich, L. Perera, M. L. Berkowitz, O. Cheshnovsky, *J. Chem. Phys.* **1996**, *105*, 2675.
32 X. B. Wang, X. Yang, J. B. Nicholas, L. S. Wang, *Science* **2001**, *294*, 1322.
33 J.-W. Shin, N. I. Hammer, E. G. Diken, M. A. Johnson, R. S. Walters, T. D. Jaeger, M. A. Duncan, R. A. Christie, K. D. Jordan, *Science* **2004**, *304*, 1137.
34 M. Miyazaki, A. Fujii, T. Ebata, N. Mikami, *Science* **2004**, *304*, 1134.
35 J. M. Headrick, E. G. Diken, R. S. Walters, N. I. Hammer, R. A. Christie, J. Cui, E. M. Myshakin, M. A. Duncan, M. A. Johnson, K. D. Jordan, *Science* **2005**, *308*, 1765.
36 J. M. Weber, J. Kim, E. A. Woronowicz, G. H. Weddle, I. Becker, O. Cheshnovsky, M. A. Johnson, *Chem. Phys. Lett.* **2001**, *339*, 337.
37 A. E. Bragg, J. R. R. Verlet, A. Kammrath, O. Cheshnovsky, D. M. Neumark, *Science* **2004**, *306*, 669.
38 D. H. Paik, I.-R. Lee, D.-S. Yang, J. S. Baskin, A. H. Zewail, *Science* **2004**, *306*, 672.
39 J. R. R. Verlet, A. E. Bragg, A. Kammrath, O. Cheshnovsky, D. M. Neumark, *Science* **2005**, *307*, 93.
40 C. Steinbach, P. Andersson, J. K. Kazimirski, U. Buck, V. Buch, T. A. Beu, *J. Phys. Chem. A* **2004**, *108*, 6165.
41 H. Saigusa, E. C. Lim, *J. Phys. Chem.* **1995**, *99*, 15738.
42 P. Benharash, M. J. Gleason, P. M. Felker, *J. Phys. Chem. A* **1999**, *103*, 1442.
43 F. Piuzzi, I. Dimicoli, M. Mons, P. Millie, V. Brenner, Q. Zhao, B. Soep, A. Tramer, *Chem. Phys.* **2002**, *275*, 123.
44 J. K. Song, S. Y. Han, I. Chu, J. H. Kim, S. K. Kim, S. A. Lyapustina, S. Xu, J. M. Nilles, K. H. Bowen, Jr., *J. Chem. Phys.* **2002**, *116*, 4477.
45 T. Beitz, R. Laudien, H.-G. Löhmannsröben, B. Kallies, *J. Phys. Chem. A* **2006**, *110*, 3514.
46 M. Mitsui, A. Nakajima, K. Kaya, U. Even, *J. Chem. Phys.* **2001**, *115*, 5707.
47 M. Mitsui, A. Nakajima, K. Kaya, *J. Chem. Phys.* **2002**, *117*, 9740.
48 M. Mitsui, S. Kokubo, N. Ando, Y. Matsumoto, A. Nakajima, K. Kaya, *J. Chem. Phys.* **2004**, *121*, 7553.
49 M. Mitsui, Y. Matsumoto, N. Ando, A. Nakajima, *Eur. Phys. J. D* **2005**, *34*, 169.
50 M. Mitsui, Y. Matsumoto, N. Ando, A. Nakajima, *Chem. Lett.* **2005**, *34*, 1244.
51 M. Mitsui, N. Ando, S. Kokubo, A. Nakajima, K. Kaya, *Phys. Rev. Lett.* **2003**, *91*, 153002.
52 U. Even, J. Jortner, D. Noy, N. Lavie, C. Cossart-Magos, *J. Chem. Phys.* **2000**, *112*, 8068.
53 G. Scoles, *Atomic and Molecular Beam Methods*, Oxford University Press, New York, Oxford, **1986**.
54 E. R. Bernstein, *Atomic and Molecular Clusters (Studies in Physical and Theoretical Chemistry)*, Amsterdom, Netherlands, New York, Elsevier, **1990**.
55 U. Even, I. Al-Hroub, J. Jortner, *J. Chem. Phys.* **2001**, *115*, 2069.
56 A. Nakajima, T. Taguwa, K. Hoshino, T. Sugioka, T. Naganuma, F. Oho, K. Watanabe, K. Nakao, Y. Konishi, R. Kishi, K. Kaya, *Chem. Phys. Lett.* **1993**, *214*, 22.
57 J. B. Hopkins, D. E. Powers, R. E. Smalley, *J. Phys. Chem.* **1981**, *85*, 3739.
58 P. R. R. Langridge-Smith, D. V. Brumbaugh, C. A. Haynam, D. H. Levy, *J. Phys. Chem.* **1981**, *85*, 3742.
59 K. H. Fung, H. L. Selzle, E. W. Schlag, *J. Phys. Chem.* **1983**, *87*, 5113.
60 K. S. Law, M. Schauer, E. R. Bernstein, *J. Chem. Phys.* **1984**, *81*, 4871.
61 M. Schauer, E. R. Bernstein, *J. Chem. Phys.* **1985**, *82*, 3722.
62 K. O. Börnsen, H. L. Selzle, E. W. Schlag, *J. Chem. Phys.* **1986**, *85*, 1726.
63 B. W. Van De Waal, *Chem. Phys. Lett.* **1986**, *123*, 69.
64 G. D. Mistro, A. J. Stace, *J. Chem. Phys.* **1993**, *98*, 3905.
65 C. Gonzalez, E. C. Lim, *J. Phys. Chem. A* **2001**, *105*, 1904.
66 T. Iimori, Y. Ohshima, *J. Chem. Phys.* **2002**, *117*, 3656.
67 D. C. Easter, *J. Phys. Chem. A* **2003**, *107*, 2148.
68 K. Ohashi, N. Nishi, *J. Chem. Phys.* **1991**, *95*, 4002.
69 K. Ohashi, Y. Nakai, T. Shibata, N. Nishi, *Laser Chem.* **1994**, *14*, 3.
70 M. J. Rusyniak, Y. M. Ibrahim, D. L. Wright, S. N. Khanna, M. S. El-Shall, *J. Am. Chem. Soc.* **2003**, *125*, 12001.
71 P. D. Burrow, J. A. Michejda, K. D. Jordan, *J. Chem. Phys.* **1987**, *86*, 9.
72 D. E. Paul, D. Lipkin, S. I. Weissman, *J. Am. Chem. Soc.* **1956**, *78*, 116.
73 R. G. Lawler, G. K. Fraenkel, *J. Chem. Phys.* **1968**, *49*, 1126.
74 T. Shida, S. Iwata, *J. Am. Chem. Soc.* **1973**, *95*, 3473.
75 G. R. Stevenson, M. P. Espe, R. C. Reiter, *J. Am. Chem. Soc.* **1986**, *108*, 5760.
76 J. C. Moore, C. Thornton, W. B. Collier, J. P. Devlin, *J. Phys. Chem.* **1981**, *85*, 350.
77 D. R. Lide, *CRC Handbook of Chemistry and Physics*, 79th ed., CRC press, **1998–1999**.
78 S. Y. Han, J. K. Song, J. H. Kim, H. B. Oh, S. K. Kim,

J. Chem. Phys. **1999**, *111*, 4041.
79 T. Kondow, *J. Phys. Chem.* **1987**, *91*, 1307.
80 M. Knapp, O. Echt, D. Kreisle, E. R. Recknagel, *J. Chem. Phys.* **1986**, *85*, 636.
81 K. Mitsuke, T. Kondow, K. Kuchitsu, *J. Phys. Chem.* **1986**, *90*, 1505.
82 M. Armbruster, H. Harberland, H. G. Schindler, *Phys. Rev. Lett.* **1981**, *47*, 323.
83 T. Kondow, T. Nagata, K. Kuchitsu, *Z. Phys. D: At., Mol. Clusters* **1989**, *12*, 291.
84 J. K. Song, N. K. Lee, J. H. Kim, S. Y. Han, S. K. Kim, *J. Chem. Phys.* **2003**, *119*, 3071.
85 X. B. Wang, C. F. Ding, L. S. Wang, *J. Chem. Phys.* **1999**, *110*, 8217.
86 J. Schiedt, R. Weinkauf, *Chem. Phys. Lett.* **1997**, *266*, 201.
87 S. Rentsch, J. P. Yang, W. Paa, E. Birckner, J. Schiedt, R. Weinkauf, *Phys. Chem. Chem. Phys.* **1999**, *1*, 1707.
88 S. Kokubo, N. Ando, K. Koyasu, M. Mitsui, A. Nakajima, *J. Chem. Phys.* **2004**, *121*, 11112.
89 N. Ando, S. Kokubo, M. Mitsui, A. Nakajima, *Chem. Phys. Lett.* **2004**, *389*, 279.
90 T. Nakamura, N. Ando, Y. Matsumoto, S. Furuse, M. Mitsui, A. Nakajima, *Chem. Lett.* **2006**, *35*, 888.
91 B. Palpant, Y. Negishi, M. Sanekata, K. Miyajima, S. Nagao, K. Judai, D. M. Rayner, B. Simard, P. A. Hackett, A. Nakajima, K. Kaya, *J. Chem. Phys.* **2001**, *114*, 8459.
92 H. Handschuh, G. Ganteför, W. Eberhardt, *Rev. Sci. Instrum.* **1995**, *66*, 3838.
93 O. Cheshnovsky, S. H. Yang, C. L. Pettiette, M. J. Craycraft, R. E. Smalley, *Rev. Sci. Instrum.* **1987**, *58*, 2131.
94 H. Hotop, W. C. Lineberger, *J. Phys. Chem. Ref. Data* **1975**, *4*, 539.
95 T. Tsukuda, M. A. Johnson, T. Nagata, *Chem. Phys. Lett.* **1997**, *268*, 429.
96 F. A. Akin, C. C. Jarrold, *J. Chem. Phys.* **2003**, *118*, 1173.
97 E. J. Hart, J. W. Boag, *J. Am. Chem. Soc.* **1962**, *84*, 4090.
98 C. Kraus, *J. Am. Chem. Soc.* **1908**, *30*, 1323.
99 See, for example: W. J. Chase, J. W. Hunt, *J. Phys. Chem.* **1975**, *79*, 2835.
100 See, for example: R. A. Holroyd, T. E. Gangwer, A. O. Allen, *Chem. Phys. Lett.* **1975**, *31*, 520.
101 P. D. Burrow, A. E. Howard, A. R. Johnston, K. D. Jordan, *J. Phys. Chem.* **1992**, *96*, 7570.
102 A. Singh, H. D. Gesser, A. R. Scott, *Chem. Phys. Lett.* **1968**, *2*, 271.
103 I. P. Bell, M. A. Rodgers, H. D. Burrows, *J. Chem. Soc., Faraday Trans.* **1977**, *73*, 315.
104 I. A. Shkrob, M. C. Sauer, Jr., *J. Phys. Chem. A* **2002**, *106*, 9120.
105 C. Xia, J. Peon, B. Kohler, *J. Chem. Phys.* **2002**, *117*, 8855.
106 C. Desfrançois, H. Abdoul-Carime, C. Adjouri, N. Khelifa, J. P. Schermann, *Europhys. Lett.* **1994**, *26*, 25.
107 C. Desfrançois, H. Abdoul-Carime, N. Khelifa, J. P. Schermann, V. Brenner, P. Millie, *J. Chem. Phys.* **1995**, *102*, 4952.
108 J. H. Hendricks, S. A. Lyapustina, H. L. de Clercq, K. H. Bowen, *J. Chem. Phys.* **1998**, *108*, 8.
109 M. Gutowski, C. S. Hall, L. Adamowicz, J. H. Hendricks, H. L. de Clercq, S. A. Lyapustina, J. M. Nilles, S.-J. Xu, K. H. Bowen, Jr., *Phys. Rev. Lett.* **2002**, *88*, 143001.
110 C. G. Bailey, C. E. H. Dessent, M. A. Johnson, K. H. Bowen, *J. Chem. Phys.* **1996**, *104*, 6976.
111 T. Maeyama, T. Tsumura, A. Fujii, N. Mikami, *Chem. Phys. Lett.* **1997**, *264*, 292.
112 L. G. Christophorou, P. G. Datskos, H. Faidas, *J. Chem. Phys.* **1994**, *101*, 6728.
113 D. W. Arnold, C. Xu, E. H. Kim, D. M. Neumark, *J. Chem. Phys.* **1994**, *101*, 912.
114 T. Takayanagi, *Chem. Phys.* **2004**, *302*, 85.
115 M. J. Frisch, G. W. Trucks, H. B. Schlegel, G. E. Scuseria, M. A. Robb, J. R. Cheeseman, V. G. Zakrzewski, J. A. Montgomery, Jr., R. E. Stratmann, J. C. Burant, S. Dapprich, J. M. Millam, A. D. Daniels, K. N. Kudin, M. C. Strain, O. Farkas, J. Tomasi, V. Barone, M. Cossi, R. Cammi, B. Mennucci, C. Pomelli, C. Adamo, S. Clifford, J. Ochterski, G. A. Petersson, P. Y. Ayala, Q. Cui, K. Morokuma, P. Salvador, J. J. Dannenberg, D. K. Malick, A. D. Rabuck, K. Raghavachari, J. B. Foresman, J. Cioslowski, J. V. Ortiz, A. G. Baboul, B. B. Stefanov, G. Liu, A. Liashenko, P. Piskorz, I. Komaromi, R. Gomperts, R. L. Martin, D. J. Fox, T. Keith, M. A. Al-Laham, C. Y. Peng, A. Nanayakkara, M. Challacombe, P. M. W. Gill, B. Johnson, W. Chen, M. W. Wong, J. L. Andres, C. Gonzalez, M. Head-Gordon, E. S. Replogle, J. A. Pople, *Gaussian 98 (Revision A.11)*, Gaussian, Inc., Pittsburgh PA, **2001**.
116 R. Ayala, J. M. Martinez, R. R. Pappalardo, E. S. Marcos, *J. Phys. Chem. A* **2000**, *104*, 2799.
117 F. Gutmann, L. E. Lyons, *Organic Semiconductors*, Wiley, New York, **1967**.
118 E. A. Silinsh, *Organic Molecular Crystals: Their Electronic States*, Springer, Berlin, **1980**, and references therein.
119 M. Pope, C. E. Swenberg, *Electronic Processes in Organic Crystals*, Oxford Univ. Press, London, **1982**.
120 J. D. Wright, *Molecular Crystals*, Cambridge University Press, **1987**.
121 V. Čápek, E. A. Silinsh, *Chem. Phys.* **1995**, *200*, 309.
122 See, for example: N. Sato, K. Seki, H. Inokuchi, *J. Chem. Soc., Faraday Trans. 2* **1981**, *77*, 1621.
123 K. H. Frank, P. Yannoulis, R. Dudde, E. E. Koch, *J. Chem. Phys.* **1988**, *89*, 7569.
124 I. G. Hill, A. Kahn, Z. G. Soos, R. A. Pascal, Jr., *Chem. Phys. Lett.* **2000**, *327*, 181.
125 E. V. Tsiper, Z. G. Soos, W. Gao, A. Kahn, *Chem. Phys. Lett.* **2002**, *360*, 47.
126 F. Amy, C. Chan, A. Kahn, *Org. Electron.* **2005**, *6*, 85.
127 K. D. Jordan, P. D. Burrow, *Chem. Rev.* **1987**, *87*, 557.
128 This sudden spectral variation with n ranging from 56 to 60 suggests that some structural morphology transition occurs in isomer II with increasing the cluster size, the detailed interpretation of which will be presented elsewhere.
129 I. V. Brovchenko, *Chem. Phys. Lett.* **1997**, *278*, 355.
130 I. Eisenstein, R. W. Munn, *Chem. Phys.* **1983**, *77*, 47.
131 W. R. Salaneck, *Phys. Rev. Lett.* **1978**, *40*, 60.
132 D. M. Neumark, K. R. Lykke, T. Andersen, W. C. Lineberger, *J. Chem. Phys.* **1985**, *83*, 4364.
133 M. S. Johnson, K. T. Kuwata, C.-K. Wong, M. Okumura, *Chem. Phys. Lett.* **1996**, *260*, 551.
134 C. G. Bailey, J. Kim, C. E. H. Dessent, M. A. Johnson, *Chem. Phys. Lett.* **1997**, *269*, 122.
135 O. M. Cabarcos, C. J. Weinheimer, J. M. Lisy, S. S. Xantheas, *J. Chem. Phys.* **1999**, *110*, 5.
136 P. S. Weiser, D. A. Wild, E. J. Bieske, *Chem. Phys. Lett.* **1999**, *299*, 303.
137 W. Kim, M. W. Schaeffer, S. Lee, J. S. Chung, P. M. Felker, *J. Chem. Phys.* **1999**, *110*, 11264.

138 M. R. Furlanetto, N. L. Pivonka, T. Lenzer, D. M. Neumark, *Chem. Phys. Lett.* **2000**, *326*, 439.
139 T. Beitz, R. Laudien, H.-G. Löhnmannsröben, B. Kallies, *J. Phys. Chem. A* **2006**, *110*, 3514.
140 B. Bouvier, V. Brenner, P. Millié, J.-M. Soudan, *J. Phys. Chem. A* **2002**, *106*, 10326.
141 R. S. Berry, J. Jellinek, G. Natanson, *Chem. Phys. Lett.* **1984**, *107*, 227.
142 R. S. Berry, J. Jellinek, G. Natanson, *Phys. Rev.* **1984**, *30*, 919.
143 J. Jellinek, T. L. Beck, R. S. Berry, *J. Chem. Phys.* **1986**, *84*, 2783.

Award recipient

Masaaki Mitsui was born in Yamaguchi, Japan in 1971. He graduated from the Department of Chemistry, the Tokyo Institute of Technology in 1995, and received his M.Sci. (1997) under the supervision of Professor Kinichi Obi. He received his Ph.D. degree in 2000 from the Department of Chemistry, the University of Kyoto under the direction of Associate Prof. Yasuhiro Ohshima and Prof. Okitsugu Kajimoto. In 2000, he moved to the Department of Chemistry at Keio University as a Research for the Future postdoctoral fellow and worked with Prof. Atsushi Nakajima. After this, he became a research associate in Prof. Nakajima's group in 2002 and was promoted to an assistant professor in 2006. His current research interests are focused on laser spectroscopy of gas-phase clusters and surface chemistry of supported clusters.

Atsushi Nakajima was born in Tokyo. After graduation from the Faculty of Science at the University of Tokyo in 1984, he received both his Master degree in 1986 and his Doctor of Science degree in 1989 from the University of Tokyo. After getting the doctor degree, he moved to the Department of Chemistry, Keio University as a research associate in 1989. He was promoted to an associate professor in 1997 and to professor of Keio University in 2001. His research interests are in nano-scale cluster science, laser chemistry, and chemical reaction dynamics, especially in the designed creation of nano-cluster-based materials. He received the Chemical Society of Japan (CSJ) Award for Young Chemists in 1995. He is the vice chair of the Physical Chemistry Division in CSJ and is the vice president of Japan Society of Molecular Science.